UNIVERSITY OF THESSALY

SCHOOL OF ENGINEERING

DEPARTMENT OF MECHANICAL ENGINEERING

FLOW AND PERMEABILITY THROUGH FIBROUS MEDIA

by

CHRISTINA MANTI

Submitted in partial fulfillment of the requirements for the degree of Diploma in Mechanical Engineering at the University of Thessaly

Volos, February 2022

UNIVERSITY OF THESSALY

SCHOOL OF ENGINEERING

DEPARTMENT OF MECHANICAL ENGINEERING

FLOW AND PERMEABILITY THROUGH FIBROUS MEDIA

DIPLOMA THESIS

ACADEMIC YEAR: 2021-2022

by

CHRISTINA MANTI

Submitted in partial fulfillment of the requirements for the degree of Diploma in Mechanical Engineering at the University of Thessaly

Volos, February 2022

Approved by the Committee on Final Examination:

Advisor	Dr Athanasios Papathanasiou, Professor, Department of Mechanical Engineering, University of Thessaly
Member	Dr Georgios Haralampous, Assistant Professor, Department of Mechanical Engineering, University of Thessaly
Member	Dr Georgios Saharidis, Associate Professor, Department of Mechanical Engineering, University of Thessaly

Date Approved: [February 25, 2022]

ACKNOWLEDGEMENTS

With the elaboration of the diploma thesis and the completion of my undergraduate studies in the Department of Mechanical Engineering of the University of Thessaly, I would like to thank some people who contributed significantly to the realization of my goal. First of all, I would like to express my deepest appreciation to my supervisor professor of my thesis Dr Athanasios Papathanasiou, for the trust he showed me, for his invaluable help and for our perfect cooperation throughout my undergraduate studies. Also, I am very grateful cooperating with Dr Andreas Tsiantis for his guidance as well as his willingness to answer my questions easily, especially for the OpenFoam. Also, I would like to thank the other members of the three-member committee, for the time and attention they showed. Finally, I owe the biggest thanks to my family who is always by my side supporting my every choice, as well as to my closest people, Ioanna, Katerina and Dimitris who supported me in every difficulty and shared with them the most beautiful moments of our student years.

Manti Christina

TRANSPORT AND PERMEABILITY THROUGH FIBROUS MEDIA

MANTI CHRISTINA

Department of Mechanical Engineering, University of Thessaly

Supervisor: Dr Athanasios Papathanasiou

Professor of Operational Research in area of Energy, industrial processes and pollution abatement technology

ABSTRACT

The objective of the current thesis is to develop a model for coupled flow and diffusion in fibrous porous media. This diploma thesis includes both a literature review and a computational section.

The flow-permeability and the transport of fluids and gases through fibrous media is very critical for a lot of industries. As a result, understanding the flow phenomena and determining the permeability in fibrous porous media is essential for successful process design. For this reason, in the first section an outline of the fundamental principles, theories and correlations between significant concepts is presented.

Following that, two cases of fibrous porous media are discussed and simulations are carried out with the help of the open-source package, OpenFoam, to investigate permeability and transport phenomena that are influenced by the range of the Peclet number.

For this purpose, a 2D grid with 500 fibers and a volume fraction equal to 0.2 is designed with the help of the open-source program Gmsh. As the flow is incompressible and the fluid is Newtonian, "SimpleFoam" is chosen as the most appropriate solver. Three simulations are conducted with three different diffusion coefficients in order to investigate how the response of a fibrous medium is affected by the change of the Peclet number.

Subsequently, a second case identical to the first one is presented with the only difference of a volume fraction equal to 0.4. The same procedure is used to evaluate the changes in permeability that occur as a result of a different volume fraction.

TABLE OF CONTENTS

List of Figures

Chapter 1

Introduction

1.1. Motivation

Flow through fibrous (porous) media is a problem of long-standing interest in engineering due to its importance in the manufacturing and process industries. Also, it is of direct relevance to several composites forming operations such as liquid molding, pultrusion, and autoclave processing (Chen & Papathanasiou, 2008). The flow-permeability and the transport of fluids and gases through fibrous media is very important for a lot of industries, such us the petroleum industry, as well as engineering, geology, agriculture but also biomedical engineering and other applied sciences, such as acoustic designing for the need of recording spaces in the music industry. Furthermore, a lot of processes that we take for granted, such as filtering and heat sinks or carbon-fiber manufacturing depend greatly on the permeability of the material and a lot of research has been devoted on the subject, in order to predict the permeability of a fibrous medium (Karakashov et al, 2019). Fibrous porous media have received great attention in a wide variety of applications including fuel cells, filtration, medical science, and biological transport phenomena. To understand the transport phenomena in porous media, a necessary condition is for permeability to be measured.

Understanding the flow phenomena that take place inside the fibrous media at both the macroscopic and the microscopic length scales is critical to successful process design. Therefore, flow simulation tools are being increasingly used for this purpose and a great deal of effort has been given to developing theoretical models for calculating the permeability in fibrous porous media (Chen & Papathanasiou, 2007).

1.2. Definitions

According to Fidjestol and Lewis (1998) Permeability refers to the measuring of how easily a liquid or a gas is able to flow through a material. The measure of that ease is described by a property of the material called Permeability and it is determined by the depth of the penetration or the amount of liquid or gas or chemical substance that is able to pass – permeate through the sample material. There are two reasons why permeability is important, the first one is to calculate how quickly a substance will enter and flow through the sample material and the second is how quickly the substance can be extracted from the material (Fidgestol & Lewis, 1998).

Krishan Chawla offers a more comprehensive description of what a fibrous material is, in his 2016 ‘’Fibrous Materials’’ book. He writes that fibers are extremely important in the manufacturing industry and are separated to natural and synthetic. Natural fibers are also separated to organic and inorganic; some organic fibers include cotton or wool while some natural inorganic fibers include asbestos and basalt.

1.3. Scope of Current Work

The present diploma thesis was conducted as a combined literature study of the basic concepts of permeability and transport through fibrous media and a computational part including simulations with the help of the open-source package, OpenFoam.

For this reason, basic principles, theories as well as relationships between important concepts (i.e., porosity/permeability) are presented in order to provide a better understanding.

Subsequently in the computational study, two cases of flow in fibrous porous media are analyzed for a range of the pertinent parameter, namely the Peclet number.

1.4. Outline of Remaining Chapters

In the following, a literature review is given in the next Chapter {2}. Basic concepts, methods, and theory, covering the fundamentals are presented in this section of the thesis.

Subsequently, previous research, numerical models used in previous works and results are given in Chapter {3}.

This is followed by Chapter {4} which constitutes the computational part in which a Newtonian-viscous flow model is described, and a flow simulation tool is being used for this purpose. The response of a fibrous medium is investigated and how it is affected by the change of the Peclet number.

Finally, in the last subsection of the computational part conclusions and a future work are presented.

CHAPTER 2

Background & Basic Concepts

2.1. Methods for describing the Permeability of Fibrous Materials

2.1.1. Darcy's Law

The first scientists to study the property of permeability was Henry Darcy in 1855, measuring the permeability of water through sand, and using his experiments and empirical evidence to form the law of Darcy:

$$(V_j)_f = -\frac{K^{(j)}}{\mu} \cdot \frac{\partial}{\partial x_j}\left[(\bar{p})_f\right]^f \quad \textit{Equation 1}$$

Where:

$K^{(j)}$: Permeability of porous medium at direction [m^2].

$(V_j)_f$: Fluid phase volume average of velocity of injected flow at j direction. [m/s]

μ : Dynamic viscosity of the fluid. [kg/m*s]

$\left[(\bar{p})_f\right]^f$: Fluid intrinsic volume average of injection pressure. [N/m^2]

2.1.2. Early Methods

Some early methods for measuring permeability in fibrous materials can be found in Gebart and Lindstorms in polymer materials (1996):

Any method for permeability measurements that is applied must be relatively easy to perform and analyze and as a result, the majority of the approaches documented in the literature are either radial flow or parallel flow type. These strategies can be tweaked in a variety of ways. The usage of a stable flow front or a flowing flow front are two examples of such variations.

There are three methods usually applied for measuring effective permeability (k_{eff}^{θ}) in a given direction with a θ angle to the global coordinate system as referred in the (Gebart & Lidström, 1996). The first two methods use parallel flow in a rectangular mold, with the distinction being whether the flow is transient with a moving flow front or stationary with saturated reinforcement. The third method involves injecting liquid into the middle of a flat mold and watching the radial flow that results.

In the two parallel flow approaches, three different experiments are required, however for the radial flow method, only one experiment is required. The below equations present the formulas for measuring the effective permeability using the three different methods (Gebart & Lidström, 1996).

- For a parallel flow, saturated reinforcement,

$$k_{eff}^{\theta} = \frac{Q*\mu*L}{A*\Delta p} \qquad \textit{Equation 2}$$

- For a parallel flow, moving flow front

$$k_{eff}^{\theta} = \frac{\mu*(1-V_f)}{2*\Delta p} B_1 \qquad \textit{Equation 3}$$

- For a radial flow,

$$k_{eff}^{\theta} = \frac{\mu*(1-V_f)}{\Delta p} \frac{1-\alpha}{\alpha} {R_o}^2 B_2 \qquad \textit{Equation 4}$$

Where, the constants B_1 and B_2 are slopes in least-squares fits of functions of flow-front position vs. time and V_f is the fiber volume. Further analysis of how these methods and calculations are applied is presented in the (Gebart & Lidström, 1996).

Experimental results and error analysis found in Gebart and Lidström in polymer materials (1996), have shown that none of these methods are better than the others, however a larger deflection of the mold was observed with the radial flow method.

2.2. Basic Concepts of Porous Media Theory

A porous medium is a partition of space into a solid matrix, M, and a porous matrix, P, such that any point in space, x, is either part of the solid ($x \in M$) or the porous matrix ($x \in P$) (Hilfer, 1996). The boundary between porous matrix and solid matrix is denoted as Γ. The porous matrix, or pore space, is assumed to be saturated with a carrier fluid, while the solid matrix is occupied by a solid substance. The carrier fluid is required not to penetrate the solid, and the solubility of the tracer in the solid is assumed to be zero. In other words, both carrier fluid and tracer will be found in the porous matrix only. Since the properties of both the carrier fluid and the tracer differ so strongly in the solid and the porous matrix, the geometric characteristics of the porous medium, like its symmetry and connectivity will have a large impact on the transport properties of the porous medium. To quantify the geometric properties of a given porous medium, it is customary to introduce the characteristic function, χ, such that:

$$\chi(x) = \begin{cases} 1 & if\ x \in P \\ 0 & else \end{cases} \qquad \textit{Equation 5}$$

One of the most important quantities in the theory of porous media is, the porosity, φ, defined by:

$$\varphi(V,x) = \frac{1}{V}\int_V \chi(x)dx, \qquad \textit{Equation 6}$$

where V denotes a sample of volume V, centered at position X. The porosity of a sample is thus the ratio of pore volume to sample volume. When evaluated on samples of small volume, the porosity necessarily fluctuates strongly with position. This observation suggests the introduction of the local porosity distribution as a function that measures the probability that a sample of given volume (or length) has a certain porosity. For samples of large volume, the fluctuations of the local porosity may decay, and a large-scale limit be obtained. In that case, the porous medium is said to be homogenous. Homogeneity of a porous medium involves a characteristic length, L, on which fluctuations of the properties of a sample of the porous medium (like porosity) become negligible. This length can usually be identified as a typical size of the grains of the solid matrix, a typical pore size, or the correlation length of the two-point correlation function.

2.2.1. Porosity and Permeability relationship in fibrous materials

To control the permeability of fibrous materials and generally porous materials one must consider a very important key parameter, $porosity = \frac{\text{Vpore}}{\text{Vsample}}$. In the above Vsample is the total sample volume and Vpore is the volume not occupied by solid fibers.

One of the most comprehensive investigations on the matter is Gebart's, in 1992, with a combination of theoretical, numerical and experimental investigations of the permeability of ordered arrays of fibers. Additionally, Koponen et al (1998) report that permeability of random-fibers sheets similar to paper and fabrics, is dependent on material porosity and not dependent on the placement of the fibers (whether they were randomly placed or not). These results agree with Clague et al (2000), in disordered fibrous media which resulted in empirically proving a relationship of permeability and porosity, with permeability as a function of porosity.

Fluid flow analyses in porous media are of great importance in a wide range of industrial applications including, transfer molding, filter analysis, transport of underground water and pollutants, and hydrocarbon recovery. Permeability is perhaps the most important property that characterizes porous media.

Darcy's equation (eq.1) has been used to solve a wide range of problems including flow through porous media with low Reynolds numbers. Darcy's law's applicability in modeling large-scale flow through fibrous media is no longer debatable; nonetheless, the quantitative effectiveness of this technique is highly dependent on the quality of available data for K and, more significantly, its change throughout the medium.

As presented in the (Papathanasiou, 1996), early attempts to predict the permeability of porous media with porosity resulted in the well-known Carman-Kozeny equation which has the following form for porous media containing spherical particles of radius R:

$$K = \frac{R^2}{4*k}\frac{\varphi^3}{(1-\varphi)^2} \qquad \textit{Equation 7}$$

- K, kozeny constant

If we define as m the mean hydraulic diameter, $m = \frac{\varphi V}{S}$, the ratio between the volume occupied by fluid over the surface area, the above equation becomes:

$$K = \frac{\varphi * m^2}{k} \qquad \textit{Equation 8}$$

The most obvious disadvantage of the above equation is that when applied for flow transverse to regular arrays of mono-disperse fibres, it predicts a finite, non-zero permeability at the point when individual fibres lock together forming an impermeable network (maximum packing). (Papathanasiou, 1996)

According to the original hypothesis, k should only be affected by the medium's geometrical structure. This is true for isotropic porous media with porosities ranging from 40% to 70%.

However, outside of this range, and particularly in fibre beds, it has been discovered that k is highly dependent on fibre volume fraction, fluid characteristics, and applied pressure drop (Skartsis et al., 1992).

Sangani and Acrivos (Sangani & Acrivos, 1982), Drummond and Tahir (Drummond, 1983), Gebart (Gebart, B. R.,1992), and Bruschke and Advani (Bruschke & Advani, 2017), established predictive models for the transverse permeability of idealised fibrous media consisting of uniformly spaced fibers of equal radius, R.

For the limiting situations of: (i) low porosity and (ii) high porosity, the Bruschke and Advani models were developed. The model for transverse permeability, K, for square packing of fibres is as follows:

At low porosities:

$$\frac{K}{R^2} = \frac{(1-\lambda^2)^2}{3\lambda^3} * \left(3\lambda \frac{arctan\sqrt{(1+\lambda)/(1-\lambda)}}{\sqrt{1-\lambda^2}} + \frac{\lambda^2}{2} + 1\right)^{-1} \qquad \textit{Equation 9}$$

Where:

$$\lambda = \sqrt{\frac{4(1-\varphi)}{\pi}} \qquad \textit{Equation 10}$$

At high porosities:

$$\frac{K}{R^2} = \frac{\lambda n^2}{4} * \left(ln(\lambda n) - \frac{3}{4} + \frac{1}{\lambda n^2} - \frac{1}{4\lambda n^4}\right) \qquad \textit{Equation 11}$$

Where:

$$\lambda n = \sqrt{\frac{1}{1-\varphi}} \qquad \textit{Equation 12}$$

In the low porosity zone, Gebart's model in 1992 is applied. For Newtonian fluids, it predicts that the transverse permeability will be:

$$\frac{K}{R^2} = \frac{16}{9\pi\sqrt{2}} * \sqrt{\frac{(1-\varphi)max}{1-\varphi} - 1} \quad \textit{Equation 13}$$

The indicator max denotes conditions that correspond to the maximum packing. It's worth noting that the above equations in the regime of low porosities get nearly identical answers. They both have accurate asymptotic behavior in the limit of maximum packing and are in good accord with experimental data for Newtonian fluid flow.

Furthermore as mentioned in (Papathanasiou, 1996), for a wide range of fibre volume fractions, comparison of the above models with numerical computations for Newtonian fluids has produced good correlation. However, because the theoretical derivations assume either a square or a hexagonal packing of the fibres, precise microstructural characteristics of the preform cannot be included in the projected effective permeability values.

2.3. Lattice Boltzman method (LBM) for calculating permeability in fibrous media

This method was introduced as an alternative meso-scale/continuum level modelling tool. It is based on a special version of the continuous Boltzman equation which discretizes time, space and velocities and is able to capture clear physics in a system, while using complex geometry and nanoscale physics to achieve this (Chung, 2011).

This method is able to simulate and thus predict the fluid flow through porous and fibrous media and obtain the permeability with different lattice numbers (Li et al, 2016).

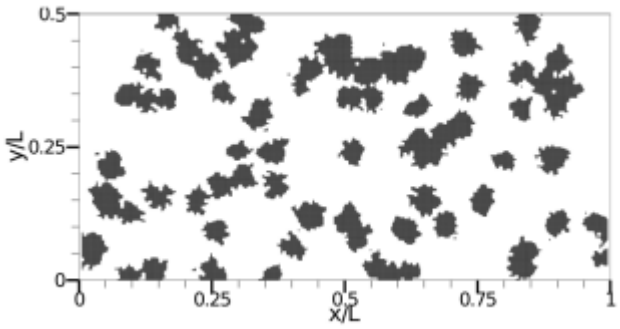

Figure 1 The 2D geometry used in the pore-scale simulation, where the symmetric boundary condition is used at the top and bottom surfaces (Li et al., 2016)

This method is extremely useful since it can predict the flow of a liquid or gas through a fibrous material without the need for any mesh generations.

2.4. Hydraulic Permeability of fibrous porous media

Darcy's law as it was described above, defines the viscous hydraulic permeability of fibrous porous media, which has been widely studied in previous years. Hydraulic permeability of flow has been predicted perpendicularly to one-dimensional circular fibers.

In Kuwabara's model in 1950 this 1D model is based on the unit cell approach and based on that, the zero vorticity of the cell has been changed to zero cell boundary shear. There have also been various numerical methods, such as the spectral boundary element formation, which is able to represent and predict hydraulic permeability in the three-dimensional models (Novacovic, 2004).

Although the research is copious in computational simulations, there haven't been a lot of analytical studies exploring the geometrical formation factors and how exactly they influence hydraulic permeability. Since superfine fibrous materials are becoming more and more relevant and more commonly used, these factors are also becoming more relevant.

2.4.1. Geometry Generation

Three different methods are commonly used to calculate hydraulic permeability of fibrous media, all with various geo-formation factors and slip effect (Shou et al., 2011):

1) Unit Cell Method
2) Voronoi Tesellation method
3) Average volume method

In the following sections we will look at the effectiveness of these methods and which ones we consider most effective.

2.4.1.1. Unit Cell Method

In order to predict the hydraulic permeability, one would need to describe the geometry of fibrous media in great detail, a feat that isn't always possible, especially with the fibrous media of quite complex nature. For this method, to make this calculation process possible, the geometrical structure of the fibrous material was assumed to be made of periodical unit cells. One-, two-, and three-dimensional systems are used in the process.

First of all, the 1D system is examined, since it is able to more intrinsically depict the nature of the system, for every fibrous media is made up of long and thin one-dimensional fibers. After this is done, then it can also be modeled 2D and 3D later.

This method will help us to have a first idea about the geometry of fibrous media. However, the information we will receive will not be 100 percent accurate.

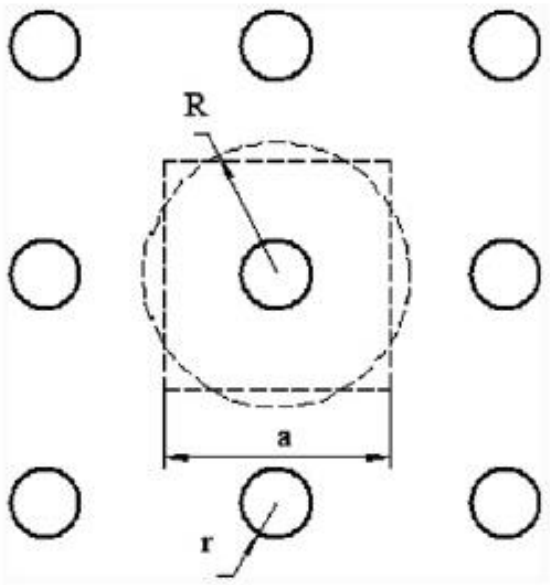

Figure 2 Unit cell (represented as a square) in a regular parallel fiber array. Source: Shou et al, 2011

2.4.1.2. Voronoi Tesellation Method

There are cases where the fibers are placed at random. This makes the flow of the unit cell a lot more complex, since the voids are now disordered and in order to visually describe the irregular and at random manner of the fiber location, a scientist may use this method.

The second method helps a lot in simulating the reality, that is, how the cells are made, as their fibers are intricately arranged and so in this way the conclusions, we will draw will be closer to reality.

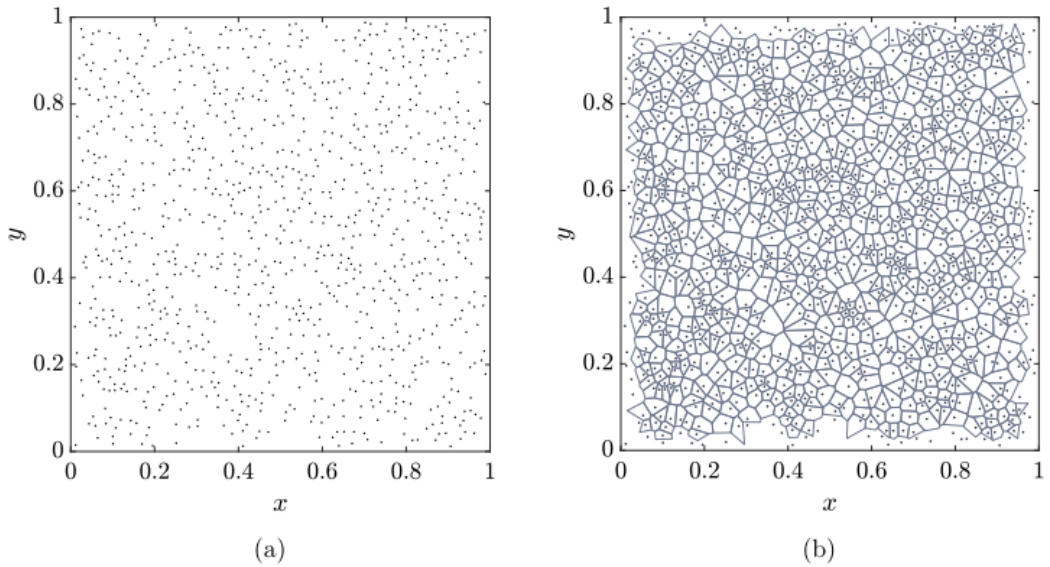

Figure 3 (a) Spatial distribution of particles, and (b) the corresponding Voronoii tesselation of the spatial distribution on the left.(Sumbekova et al., 2019)

2.4.1.3. Volume Averaging Method

In this method (Shou et al., 2011) one can examine common cases of both two and three dimensional fibrous media, which can have both various fiber orientations as well as various fiber distributions. Macroscopically speaking fiber arrangement is characterized by high anisotropic properties.

This method can determine permeability by creating a total drag in which the contribution of fibers is added in each direction. This way one can predict the transport properties of a fibrous medium on a macroscopic level; however, they must overcome a closure problem in order to determine the hydraulic permeability macroscopically within the representative elementary volume.

One can assume that a fibrous medium can consist of cubic cells which are repetitive, which represent the microscopic structure of a fibrous medium. Within every cubic cell these fibers can be located and oriented in various ways and directions, and the overall orientation of the fibers in each cubic cell can be characterized by fractions of the length of the fibers in x, y, or z axis of direction.

We notice that the third method is much more specific and we believe that it will help a lot in drawing safer conclusions than the previous methods. We believe that by combining the three methods, scientists can better understand how fibrous materials work.

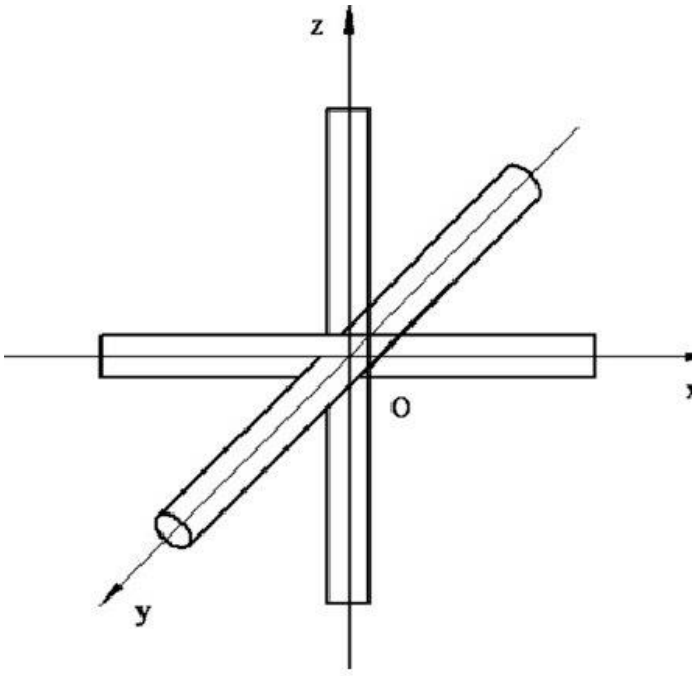

Figure 4 3D view of fibrous media based on cubic lattice. Source: Shou et al, 2011

2.5. Coupled Diffusion and Dispersion through Fibrous Media

2.5.1. Background and Motivation

All earlier studies considered that transport of solute molecules through the fibrous media occurs by diffusion only. However, when studying the dispersion of a species through a fibrous medium, many times fluid flow also contributes.

Physicists use the term dispersion as a synonym for the spreading of a distribution of mass (or energy) in a carrier medium. In the above example, the ink is dispersed in the water by diffusion. Dispersion is thus a fundamental mechanism of transport. Other examples of dispersion phenomena include the spread of sound waves and the spread of heat. Molecular diffusion is not the only mechanism that leads to dispersion. Transport by convection, for example, often leads to dispersion, too. To see this, imagine that an ink is poured into a river, and convected downstream along with the flowing water. The local velocity of the carrier will usually not be constant throughout the river but vary with position. Such velocity fluctuations introduce several different dispersion mechanisms. The interplay between dispersion and diffusion can be illustrated in the following way:

Diffusion → Dispersion ⇆ Transport ← Convection

Here, arrows should be read as 'leads to', and diffusion and convection are mentioned as examples of a dispersion- and a transport process, respectively. It is obvious that dispersion is a phenomenon of fundamental importance in daily life as well as in engineering. Consequently, there is a profound need to quantitatively understand and describe dispersion processes. Dispersion phenomena occur in a large variety of situations, and the underlying dispersive mechanisms can be of quite different nature. Flow through fixed beds is usually steady, such that the velocity of the carrier fluid at a given point does not change in time. In this case, studies on tracer dispersion can be divided into three steps: First, the geometry of the porous medium is defined. Next, the steady flow of the carrier in the porous matrix is calculated. Finally, the transport of a tracer under the combined action of molecular diffusion and convection by the steady flow of the carrier is studied.

Moreover, transport by diffusion and convection is an interesting phenomenon from a scientific point of view: Diffusion is a stochastic process, that is, a diffusing particle has no memory about its position at earlier times. Consequently, the process of diffusion is irreversible in time. In contrast, convection is a deterministic, and (under certain restrictions) completely reversible process. The interplay of two processes so different in nature leads to remarkable phenomena, some of which are discussed in this thesis. Finally, it will be seen that tracer dispersion is relatively simple to access theoretically. Consequently, a number of analytical results exist, and can be checked against the results of experiments and simulations.

2.5.2. The Convection-Diffusion Equation

We start the discussion on microscopic scales, that is, length scales smaller than the characteristic length l of the porous medium. These length scales are, however, assumed to be large compared to molecular scales, so that the carrier fluid and the tracer can be discussed in the frame of continuum mechanics. The derivation of the transport equation relies on the principle of conservation of tracer particles. One obtains the partial differential equation: (Lawley, 2007)

$$\frac{\partial c}{\partial t} = -\nabla \cdot (\boldsymbol{u}c) + \boldsymbol{D_m}\nabla^2 c \qquad \textit{Equation 14}$$

where $c(x,t)$ the local molecular concentration, D_m is the molecular diffusion coefficient, $\boldsymbol{u}(x,t)$ is a single valued vector function that measures the local fluid velocity at position x and time t. Equation (14) is called *convection-diffusion equation* since it describes the transport of a tracer under the influence of convection and molecular diffusion. It is instructive to cast Eq. (14) into dimensionless form by non-dimensionalizing all involved quantities according to:

$$\boldsymbol{u} \to \boldsymbol{u}/U, \qquad x \to x/l, \qquad t \to tU/l, \qquad c \to cl^3,$$

where U is a characteristic flow velocity. In these dimensionless variables Eq. (14) takes the form:

$$\frac{\partial c}{\partial t} = -\nabla \cdot (\boldsymbol{u}c) + \frac{1}{Pe}\nabla^2 c \qquad \textit{Equation 15}$$

The quantity:

$$\boldsymbol{Pe} = \frac{\boldsymbol{Ul}}{\boldsymbol{D_m}} \qquad \textit{Equation 16}$$

is the Peclet number and compares a typical time scale of diffusion (l^2/D_m) to a typical time scale of convection (l/U). In the next subsection more information about the Peclet number will be presented.

2.5.3. Peclet number

In many investigations, it's required to describe groundwater flow and solute transport in porous media with low permeability, where the rate of transfer owing to flow (convection) is similar to the rate of transport due to diffusion. Groundwater flow in these low-permeability environments appears to influence the evolution of certain hydrologic, geologic, and geochemical systems, as well as the buildup of petroleum and ores. It also appears to play a role in the structural evolution of areas of the crust. In the context of garbage disposal, such

ecosystems are also critical (Neuzil, 1986). Modeling of the hydrogeology of low permeability rocks surrounding nuclear waste disposal sites and landfills are good examples.

In general, convection and diffusion are considered simultaneously when simulating transport in porous media. Transport may be dominated by diffusion at low flow velocities, but advection may be dominant at high velocities. In either case, a transport model that ignores relatively minor terms is easier to implement than one that considers all transport mechanisms simultaneously, especially if the model is three-dimensional and/or includes simultaneous consideration of multiple and reactive chemical species or parameter optimization routines (Garges and Baehr, 1998). As a result, if the medium has a low permeability, it's worth seeing if advection should be considered. If not, diffusion alone can be used to mimic transport. The head and permeability distribution are not necessary for transport simulation in this situation, therefore the computation time can be reduced.

A Peclet number-based criterion is frequently used to determine if advection transport should be included. A Peclet number is a dimensionless number that can be used to compare the effectiveness of mass movement by advection to mass transfer via dispersion or diffusion (Fetter, 1999). For Peclet numbers less than 1, diffusion is usually considered the major transport mode. Unfortunately, there are up to ten alternative definitions of the Peclet number in the literature, and these multiple meanings result in highly different Peclet number values for a given situation. As a result, ignoring advection based only on a Peclet number value less than 1 does not appear to be warranted for every extant Peclet number definition.

Diffusion is consequently much'slower' than convection at large Pe, and convection dominates the transport process. Convective transport, on the other hand, is minimal when Pe is tiny compared to diffusive transfer. Convective and diffusive transport processes are linked by the Péclet number. It's linked to the Prandtl number, which relates momentum and thermal transport, and the Reynolds number, which ties inertia and viscous forces together. The Péclet number is calculated as follows:

$$\mathrm{Pe} = \frac{\text{convection transport}}{\text{diffusion transport}} = \frac{uL_{char}}{D}.$$

A second widely used formulation of the Péclet number links convective and heat transmission. It is defined as follows:

$$\mathrm{Pe} = \frac{\text{convection transport}}{\text{heat transport}} = \frac{uL_{char}}{\lambda}.$$

The Péclet number, like the Reynolds number, is not a material constant because it is dependent on both the velocity of the flow field and the system's characteristic length L char.

Literature contains a wide range of Peclet number definitions. The fundamental distinction between them is in the assumptions regarding solute transport that they are based on. Different Peclet number definitions come from different simplifications of the general solute transport equation. The effective porosity n_e, which is the porosity available for fluid flow or advection (Fetter, 2001), and the diffusion accessible porosity n, which is the fraction of the

total water filled porosity that is available for diffusive transport, are distinguished in the general form of the solute transport equation (Horseman et al., 1996). Because the diffusion accessible porosity contains a fraction of the immobile water porosity, it may be bigger than the effective porosity. As a result, one porosity may be required for calculating advection velocity while another may be necessary for determining the rate of mass buildup. Instead of using two porosity variables, advective-dispersive transport analysis has traditionally used a single lumped value of porosity (Zheng and Bennett, 2002).

2.5.4. The Navier-Stokes Equation

The principles of conservation of mass and momentum lead to the continuity and Navier-Stokes equations:

$$\frac{\partial \rho}{\partial t} + \nabla \cdot (\rho \boldsymbol{u}) = \mathbf{0} \qquad \textit{Equation 17}$$

$$\rho \left[\frac{\partial \boldsymbol{u}}{\partial t} + (\boldsymbol{u} \cdot \nabla)\boldsymbol{u}\right] - \nabla \cdot \boldsymbol{\Sigma} = \boldsymbol{f} \qquad \textit{Equation 18}$$

where ρ is the density of the fluid, Σ denotes the stress tensor, and $\boldsymbol{f}$ the externally applied force per unit volume, or body force. To process these equations further, a constitutive relation for the stress tensor must be supplied. In Newtonian fluids, for example, the stress tensor is a linear function of the velocity gradient, and Newton's law is valid:

$$\boldsymbol{\Sigma} = -\boldsymbol{p}\boldsymbol{l} + 2\boldsymbol{\mu}\boldsymbol{R}, \qquad \textit{Equation 19}$$

where p is the pressure, l the identity tensor, λ and μ are the two coefficients of viscosity, and $R = \frac{\{\nabla \boldsymbol{u}\} + \{\nabla \boldsymbol{u}\}^T}{2}$ denotes the tensor of rate of strain. Equation (18) is readily cast into dimensionless form by non-dimensionalizing all involved quantities with the characteristic length / and the characteristic velocity U according to:

$$x \to x/l, \qquad \boldsymbol{u} \to \boldsymbol{u}/U, \qquad t \to tU/l, \qquad p \to p/(U^2\rho), \qquad f \to fl/(U^2\rho).$$

In dimensionless variables Eq. (18) takes the form:

$$\frac{\partial \boldsymbol{u}}{\partial t} = -\nabla \boldsymbol{p} - (\boldsymbol{u} \cdot \nabla)\boldsymbol{u} + \frac{1}{Re}\nabla^2 \boldsymbol{u} + \boldsymbol{f} \qquad \textit{Equation 20}$$

where the quantity:

$$Re = \frac{\rho U l}{\mu}$$

is called the *Reynolds number*. Like the Peclet number, the Reynolds number is an important dimensionless quantity that allows one to distinguish between different flow regimes, as discussed below. When the left-hand side of eq. 18 vanishes, the flow is referred to as steady. In this case, the velocity at any given position is constant in time. Steady state flows

are often encountered in flow in porous media, since the forces that drive the flow change very slowly in time.

The Reynolds number is one of the most important dimensionless quantities in fluid mechanics. It correlates the inertia forces to the viscous forces. The Reynolds number was first described by Reynolds in 1883, although others have used the quantity before, e.g., Stokes. It is defined as:

$$Re = \frac{\text{inertia forces}}{\text{viscous forces}} = \frac{\rho u L_{char}}{\eta} = \frac{u L_{char}}{\nu}.$$

The Reynolds number is important for describing the transport properties of a fluid or a particle moving in a fluid. As an example, for very small organism, e.g., bacteria, the Reynolds number is very small, typically in the range of 1×10^{-6}. Given the small dimensions, these objects do not have a significant inertia and are thus mainly driven by the viscous forces of the fluid. As the objects grow larger, their inertia starts to dominate over the viscous forces. For most fish, the Reynolds number is in the range of 1×10^{5}, for a human it is in the range of 1×10^{6}.

CHAPTER 3

Previous Research

3.1. Permeability of Fibrous Biomaterials

3.1.1. The objective

One important application of fibrous media permeability is in biomedicine, as was mentioned above. Collagen is the single most important structural protein in the human body, and it is located in the extracellular space of various connective tissues. This protein is being examined here due to its fibrous nature and the fact that it is the main component of the extra-cellular matrix (DeFrates et al, 2018).

Collagen fibers are formed from collagen fibrils that have been hierarchically aggregated measuring between half to three μm in diameter (Novacovic et al, 2004). When a human joint is stressed and strained beyond its natural range of movement then a tear in the ligament might occur, or worse, a rupture. The flow of fluid, in this case, through the ligament tissue, is a very important factor in the nutrient absorption rate of the cell and the metabolic rate of the waste removal process (Novacovic et al, 2004).

Studies have been made to assess the flow inside the ligaments and describe the behavior of these biological fluids through the fibrous media of a human ligament. In order to be able to study the flow of these fluids a rheological fluid model was adopted in this biological application of previous numerical models.

Erisken, Papathanasiou, Tsiantis and Karvelas (Erisken et al., 2020) studied the permeability of ligament tissue with a computational study on healthy and injured tissues in 2020. In their study they used a biological application of a previous numerical model to study the effect the collagen fibril diameter has on distribution, and they also studied the hydraulic permeability of healthy and injured tissue comparatively, specifically in the ACL tissue (Anterior Cruciate Ligament). They hypothesized that due to the injury on the ligament the tissue became distorted in structure and as such its permeability would change through the ECM (extra cellular matrix). They hoped to use this research to understand the nature of injuries and aid in the future healing process of the ligament, which would demand the contribution of several factors such as cell function and their contribution to healing as well as regulators of the human cells like medical substances, drugs and biomolecules that would act as growth factors.

In order to enhance and better the delivery of said substances and biomolecules and control them, and in order to make them more efficient and potent and promote healing as well as increase healing speed and quality, one would first need to understand and define the flow patterns.

3.1.2. The method

Their methodology was of quite some interest, they used TEM (Transmission Electron Microscopy) in order to obtain results that would show the collagen fibril diameter as well as the diameter distribution through the images of sectioned ACL tissues. Of course, these tissues were bovine but the morphology and topology of human and bovine tissue are surprisingly alike and their research could very well have human application.

A specimen of 1 cubic mm was obtained from the middle of the tissue section and used for TEM characterization. With a uniaxial material testing machine, the researchers created injured specimens by attaching the tibia-ACL-Femur joint to the machine and stretching it until failure at a rate or 5mm/min, which is the most common physiological strain for ligaments/tendons.

They measured the collagen filament diameter and the diameter distribution by placing ten parallel lines of equal distance on the TEM image and they measured the diameter of the fibrils which intersected said lines.

As in all areas of our lives, nature teaches us and gives us answers to almost every question of our lives as we study it. So here, in the case of collagen, we realize how perfect the human body is, as scientists have been able to understand how it is made, so that fluids can penetrate tissues. As we know, every human creation copies nature. So, in this case, we hope that this component of our body, will give the answers needed to create human fibrous materials through which liquids and gases can flow comfortably.

A solution method was used for evaluating the flow of the micropolar fluid through the filament arrays:

$$(\hat{\boldsymbol{u}} \cdot \boldsymbol{\nabla})\hat{\boldsymbol{u}} = -\boldsymbol{\nabla p} + \frac{1}{Re}\boldsymbol{\nabla}^2\hat{\boldsymbol{u}} + \frac{m}{Re}\boldsymbol{\nabla} \times \boldsymbol{\omega} \qquad \textit{Equation 21}$$

$$\frac{JN}{m}\hat{\boldsymbol{u}} \cdot \boldsymbol{\nabla\omega} = \frac{1}{Re}\boldsymbol{\nabla}^2\boldsymbol{\omega} + \frac{N}{Re}\boldsymbol{\nabla} \times \hat{\boldsymbol{u}} - 2\frac{N}{Re}\boldsymbol{\omega} \qquad \textit{Equation 22}$$

uˆ = velocity vector

ω= micropolar velocity vector

*Both of these are scaled to the average velocity of the cross section

Re = Uref Reynolds number

N= gradient viscocity

m= vortex viscocity

*these three are non-dimensional parameters and they are defined as following, with L being the characteristic length of the flow path and ρ being the micropolar fluid density:

$$Re = \frac{\rho U_{ref} L}{\mu_v + k_v}, \qquad N = \frac{k_v L^2}{\gamma}, \qquad m = \frac{k_v}{\mu_v + k_v}$$

All the other parameters were made non-dimensional and were expressed with the following:

$$\hat{u} = \frac{u}{U_{ref}}, \qquad \hat{\omega} \rightarrow \frac{\omega L}{U_{ref}}, \qquad p \rightarrow \frac{p}{\rho U_{ref}^2}, \qquad J \rightarrow \frac{j}{L^2}$$

*ω=micropolar velocity component,

P= pressure

J= micro inertia constant

3.1.3. Results of the study

Using the solution of the equations mentioned above they managed to calculate and compare/contrast the hydraulic permeability of healthy and injured ligament tissue, always with consideration of the Newtonian and the micropolar fluids.

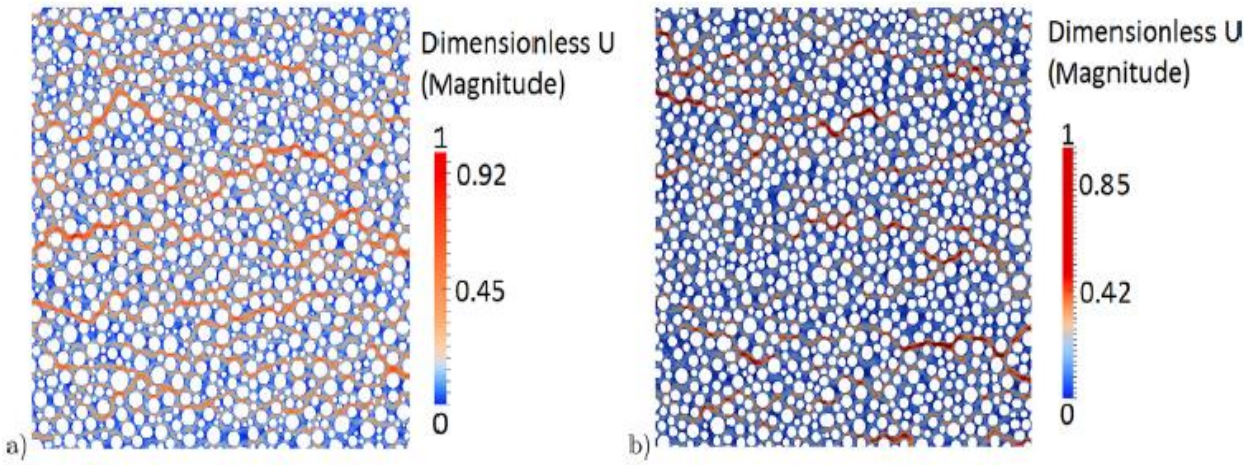

Figure 5 U= Dimensionless fluid speed, as scaled by the division of maximum velocity for a case of micropolar under m,N=10. a) Healthy and b) injured tissue, with red = high velocity and blue = low velocity Source: Erisken et al, 2020

In figure below, the researchers found an increase in hydraulic permeability in healthy ligament of 0.75%, as well as observed an increase of the values of the micropolar parameters in the cases of injured ligament. In the injured ligament tissue, there was only a very slight increase of hydraulic permeability.

With m and N = 1, it was found that the permeability of healthy ligament tissue was 10.9% higher when compared with the corresponding permeability of the injured tissue and the more the values of the micropolar parameters increased so did the permeability, when they were increased m, N = 5 and 10 then the increase of permeability was 12.4 % and 13%.

In the Newtonian case respectively the rise in hydraulic permeability in both healthy and injured ligament tissue was 11.3 %.

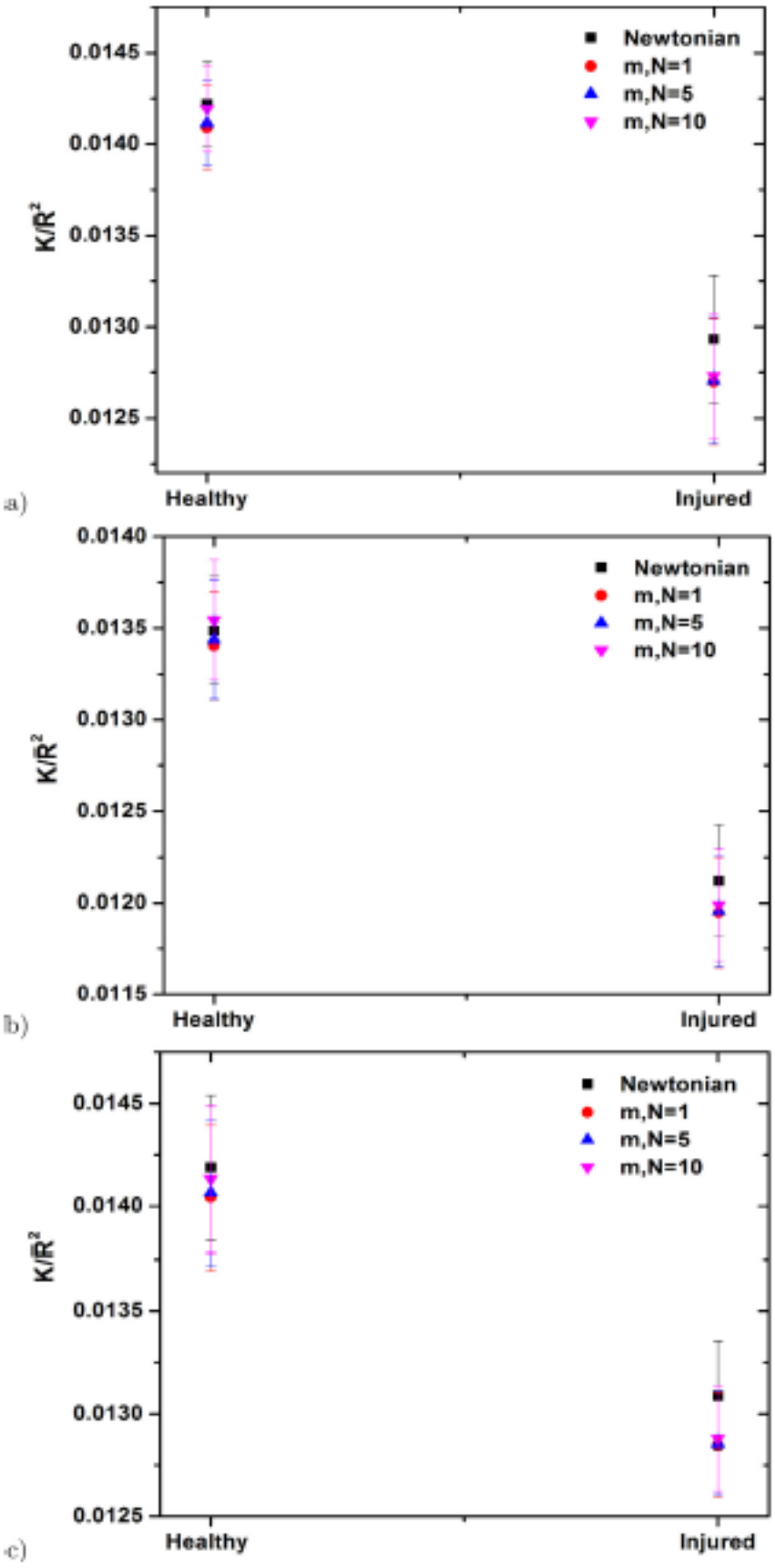

Figure 6 Hydraulic Permeability for Newtonian and micropolar cases under different random distributions for healthy and injured tissue

3.2. Effect of micropolar fluid properties on the hydraulic permeability of fibrous biomaterials

In the next section, we will consider a method to look at the effects of the properties of micropolar fluids on the hydraulic permeability of fibrous media.

3.2.1. The objective

In 2020 Papathanasiou, Tsiantis and Karvelas carried out a study to explore the effect of the micropolar fluid parameters on the hydraulic permeability of fibrous biomaterials. These biomaterials were comprised of square arrays of unidirectional fibrils. Specifically, they studied collagen, and the fluid flow of biofluids through collagen structures that are not described properly by the Newtonian flow model.

The researchers proposed that the best way to describe the behavior of these biofluids and their microscale structuring and microrotation is by the micropolar fluid model, based on a theory of non-Newtonian fluid dynamics.

Microfluids have nonsymmetrical stress tensor and can support couple stresses because they contain microelements and have an internal microstructure. They also can support surface and body couples and can change their shape, size or geometry and rotate on their own regardless the rotation of the fluid. These biofluids have a different effect on the dimensionless hydraulic permeability inside regularly ordered fibrous biomaterials.

3.2.2. The method

They used OpenFoam in 3-D to frame their simulations or micropolar fluid flow inside fiber arrays. The flow they studied was transverse and regularly ordered in a square fiber array. They used Gmsh as a mesh generator to create the instructed computational mesh. Their results show that as the mesh increased there was practically no difference in the computed microrotation values and as such they conducted all simulations by using 25 cells in the z-direction.

They computed the effective permeability of the unit cell through Darcy's law, as did the researchers in the other cases mentioned in this paper:

$$K_{eff} = \frac{Q(\mu_v)L}{\Delta PHW} \qquad \textit{Equation 23}$$

K_{eff}=Effective Permeability

Q=computed flowrate

ΔP=imposed pressure drop

H and L=dimensions of the unit cell in the x-y plane

W=dimension in the z direction

3.2.3. Results of the study

They validated these models for Newtonian and micropolar fluid flow as well, comparing them against other permeability models proposed in the Newtonian case and validated the micropolar flow numerical model against planar Poiseuille flow.

The results of their studies showed correlation between the values of the micropolar parameters an microrotation, more specifically when the first increased so did the second and after both values are increased then so does the velocity of the fluid as a result. Accompanying these changes is also a change in permeability, which increases alongside the other values.

As a secondary result they found that increasing the concentration of the microelements of the micropolar fluid changed the rate of the heat transfer, increasing it. Similar results of an increase in the heat transfer rate are achieved by increasing the Prandtl or the Eckert number.

Another crucial effect is the effect of the volume fraction on microrotation. When the volume fraction is increased then the microrotation for the same micropolar parameters would decrease. By having a larger space to accommodate the microfluid flow there is decreased flow resistance. Increasing the volume fraction ϕ led to an observation of increased values of micropolar parameters needed to sustain similar permeability for the micropolar model to the parameters of the Newtonian model.

They expressed the differences in hydraulic permeability between micropolar and Newtonian cases as a function of vortex, spin gradient viscosity and volume fraction.

$$\frac{\Delta K}{m} = aN + I(\phi, m) \qquad \textit{Equation 24}$$

m=Vortex

N=Spin gradient viscosity

ϕ = Volume fraction

A= Constant independent on m and N and weak function of ϕ

Summarizing, higher porosity led to higher hydraulic permeability of the fibrous biomaterial, caused by the increased bio rotation of the substructure of the micropolar fluid. Accordingly, lower porosity (decrease in the values of the vortex and the spin gradient viscosity) led to lower rates of microrotation and decrease of the hydraulic permeability, when compared to the Newtonian model.

Lower microrotation values led to a flow deceleration because of the contacts within the substructure of the micropolar fluid and the boundaries of the fibrous biomaterials examined.

3.3. Relationship between the axial flow permeability of fibrous media and the microstructure of the model

3.3.1. The objective

Xiaoming Chen and T.D. Papathanasiou conducted research in 2006 to establish a model for the axial hydraulic permeability (K||) of fibrous media that included explicit consideration of the microstructure and its variability.

The researchers investigated axial Stokes flow over many unidirectional, disordered fiber arrays in detail, each one comprised entirely of 600 fibers inserted at random.

A two-dimensional Stokes formula was used to represent Stokes flow in a continuous fibre grid in the axial direction.

The current study was driven by the need to build models that would estimate the axial permeability of a fibrous medium based on information of its composition, as a result of the expansion of more efficient and timely permeability test procedures.

Axial flow across unidirectional random fiber arrays is the difficulty researchers looking at their study. Theoretical conclusions for such arrays frequently differ significantly from practical data acquired in real fibrous media.

Thus, it is critical to look at the possibility of structure-permeability relationships in unstructured fiber arrays.

3.3.2. The method

Permeability parameters should be given at nodal locations or cell centers indicated by the area discretization approach to computationally model flow through fibrous preforms. The correctness of the permeability data provided is essential for successful analysis.

Long cylindrical fibers with their axes aligned in the z- direction and geometrical centers randomly distributed in the x–y plane constitute the fibrous media investigated.

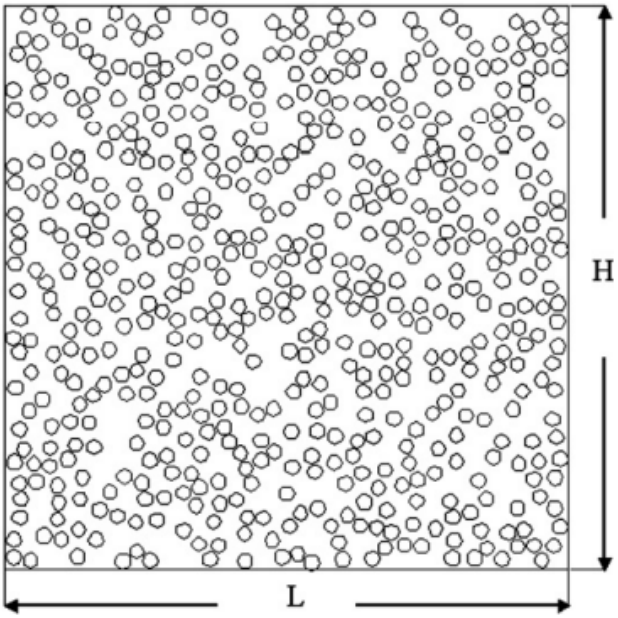

Figure 7 Representative volume for unidirectional disordered fiber arrays. (Chen & Papathanasiou, 2007)

The Stokes equations are the fundamental equations for creeping Newtonian flow through the porous media.

$$\nabla P + \mu \nabla^2 V = 0 \qquad \textit{Equation 25}$$

$$\nabla v = 0 \qquad \textit{Equation 26}$$

- P: pressure
- V: velocity vector
- μ: viscosity

The Representative Volume Elements (RVEs) used in this research were selected to represent a range of distributed fibers and created using a Monte-Carlo technique in the porosity range $0.45 < \phi < 0.90$, each constituting of 600 fibers.

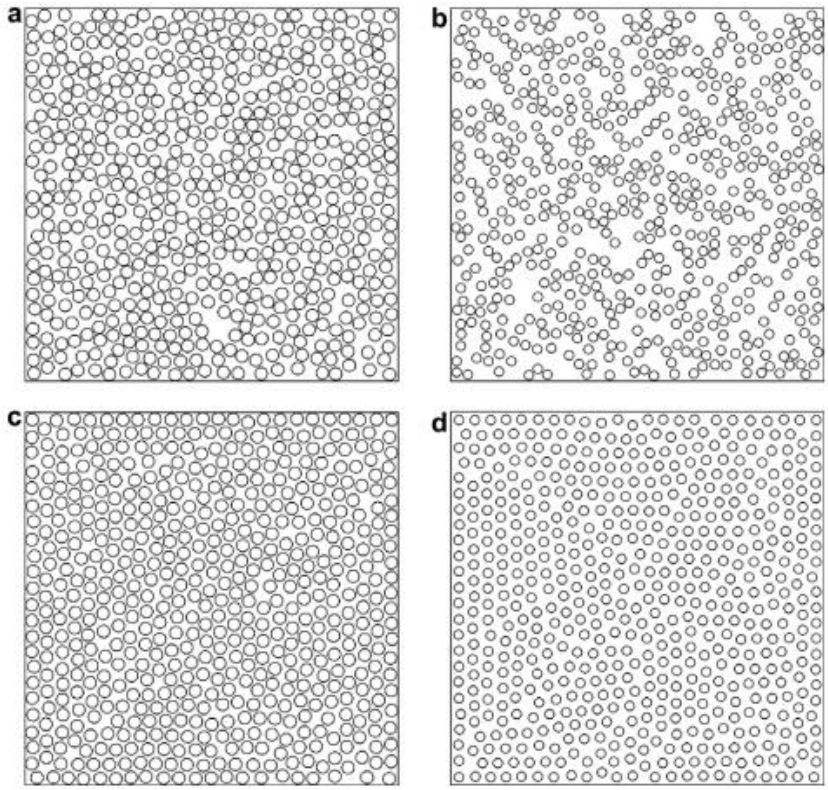

Figure 8 Typical fiber distributions generated by a Monte Carlo procedure, each with 576 fibers: (a) / = 0.5, δ_{min} = 0.1a; (b) / = 0.7, δ_{min} = 0.1a; (c) / = 0.5, δ_{min} = 0.4a; (d) / = 0.7, dmin = 1.2a (Chen & Papathanasiou, 2007)

The MC process begins with a fixed fiber packing configuration (for example, a square array) and then perturbs the fiber placements randomly and consecutively. The choice of porosity ϕ and the minimum permissible inter-fiber distance δ_{min} are the main determinants of the microstructures formed in this way.

The porosity, is estimated as: $\varphi = 1 - \frac{(N*\pi*\alpha^2)}{A}$

where N is the quantity of fibers contained, α is the fiber radius, and A is the grid's area.

The δ_{min} is the factor that prevents fibers from overlapping throughout the MC process. It is determined as the minimum permissible distance between two fiber borders.

3.3.3. Results of the study

For varying parameters of ϕ and δ_{min}, fiber distributions are illustrated in the above figure. Small δ_{min} values result in more uniform structures, whereas big δ_{min} values result in more uniform distributions. When the porosity is high, δ_{min} has a stronger effect on fiber aggregation.

By visualizing the velocity field through the fibers, the impact of fiber arrangement on the flow field may be evaluated. Flow fields estimated for axial flows through disordered fiber arrays are shown in the below figure.

Axial flow appears to be aided by the presence of big pores (or flow channels). Despite the fact that the two microstructures have the same permeability, the permeability of (a) is twice as great as that of (b).

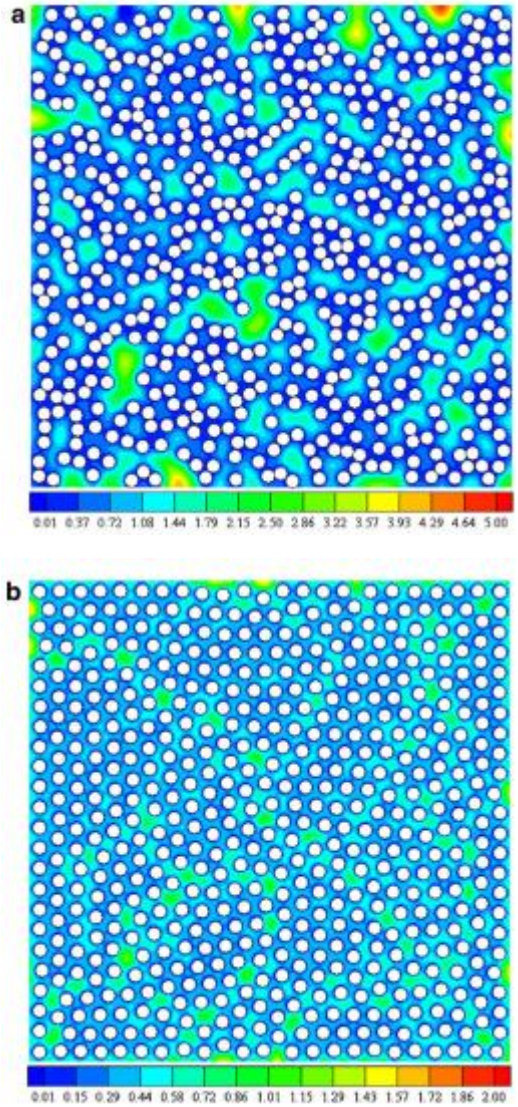

Figure 9 Contours of vz for axial flow through unidirectional disordered fiber arrays. (a) φ = 0.70, δ_{min} = 0.1a (b) φ = 0.70, δ_{min} = 1.2a (Chen & Papathanasiou, 2007)

Researchers tried to include another parameter called δ1 to decrease the error in the axial permeability estimate. This parameter defines the heterogeneity of the fiber distribution.

The result they carried out is that K|| is improved by increasing microstructure heterogeneity.

Concluding, the results show that (K||) rises as the microstructure shifts from a uniform to a non-uniform dispersion. A microstructural factor was proposed so as to define the heterogeneity of the fiber distribution and describe this relationship between (K||) and microstructure.

3.4. Variability of the Kozeny constant (kc) in flow through unidirectional fiber arrays

3.4.1. The basis

Xiaoming Chen and Thanasis D. Papathanasiou (Chen & Papathanasiou, 2006) carried out research in order to investigate saturated transverse flow over a large number of unidirectional fiber arrays and describe the wide range of the Kozeny constant values found experimentally.

The development of theoretical models for predicting permeability in porous media has taken a lot of time and effort.

Fiber arrays are typically characterized as periodic or random arrays of aligned cylinders for generating permeability simulations. Darcy's law can be used easily to determine hydraulic permeability in certain situations.

$$K = \frac{q}{H} * \frac{L*\mu}{\Delta p} \qquad \textit{Equation 27}$$

- q: flow rate
- Δp: pressure drop
- H: height of unit cell
- L: length of the unit cell

Unfortunately, it emerges that experimental data for real fiber arrays and simulated results have little association (Åström et al., 1992). This is due to the fact that permeability is a geometry-dependent feature, and the expected real fiber arrangement is rarely seen. It is commonly found in composite materials as depicted in the figure below.

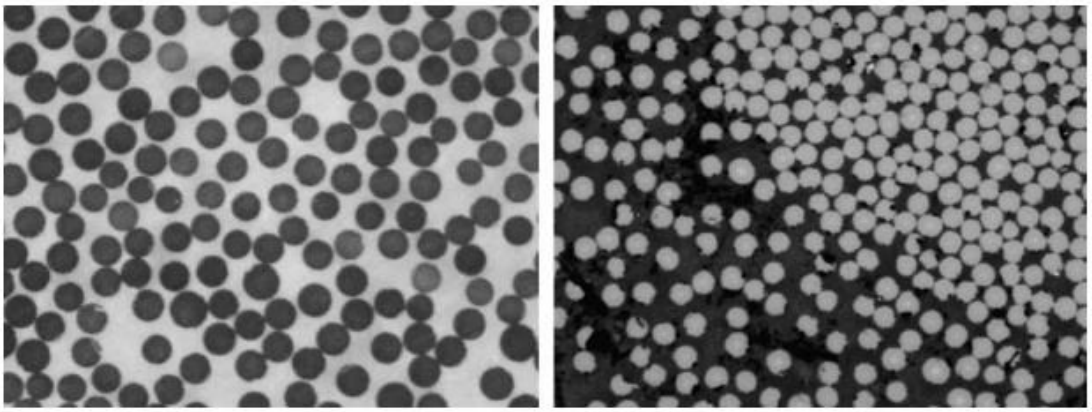

Figure 10 Typical microstructures of unidirectional laminates. (Chen & Papathanasiou, 2006)

3.4.2. The method

Using a parallel computational technique, researchers studied the effect of fiber packing statistics on the transverse permeability of random fiber arrays. Using a Monte–Carlo approach, they created a huge number of fiber distributions that are statistically homogeneous but have varying degrees of local heterogeneity. They analyzed systems with 196–900 fibers, porosity (ϕ) ranging from 0.45–0.8, and minimum inter-fiber distance (δ_{min}) ranging from 0.1R to R, R being the fiber radius. The latter variable (δ_{min}) is a crucial characteristic that determines the degree of inhomogeneity at the microscale, as we have already mentioned in the previous section (Chen & Papathanasiou, 2006).

Fiber distributions at various porosities and a different δ_{min} are shown in the figure below. It can be seen that a low δ_{min} number results in small fiber bundles, making the distribution appear more heterogeneous. With higher values of porosity, the effect Is “stronger”. On the other side, a high value of δ_{min} results in more homogeneous structures with more hexagonal arrangements.

It is good to point out that the model distributions utilized in this work, while not as complex as actual fiber arrangements, do represent a class of distributions that are more closely related to them.

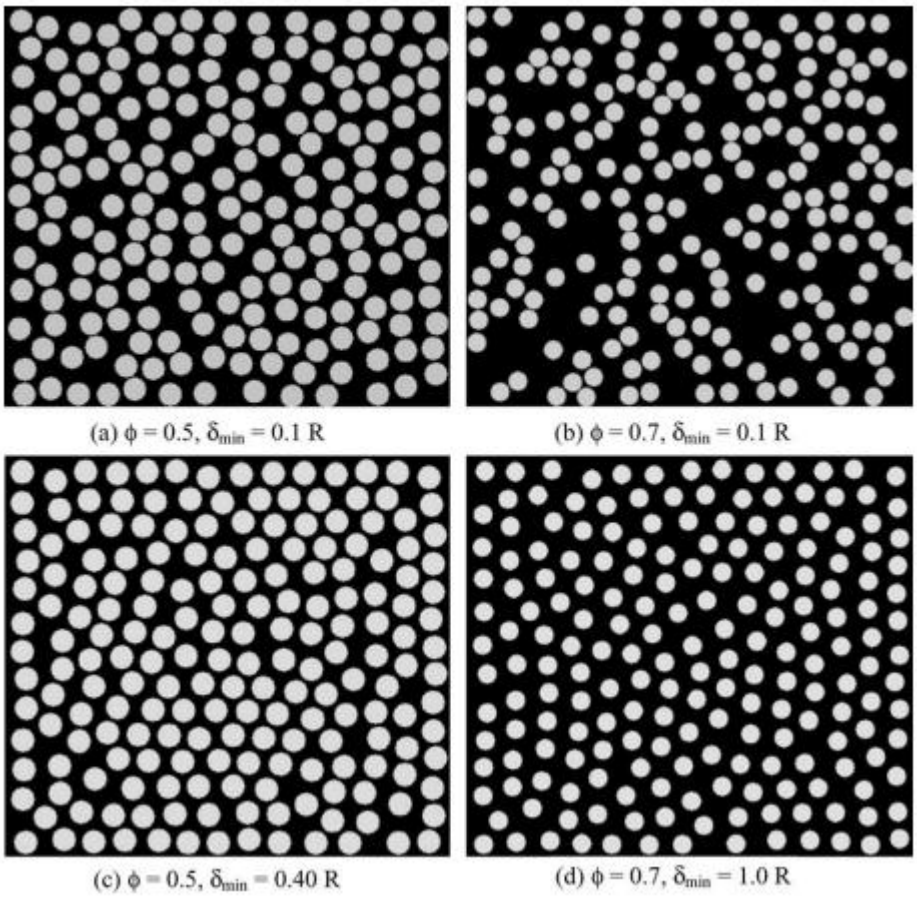

Figure 11 Typical computer-generated fiber distributions. Each image consists of 196 fiber cross sections and was generated by the MC method, starting from a 14!14 square array. (Chen & Papathanasiou, 2006)

3.4.3. Results of the study

3.4.3.1. Flow Features

It is well understood that numerical evaluations of effective characteristics based on small systems differ significantly from those relying on bigger systems, implying that the fiber distribution becomes more homogeneous as the system grows.

The below figures taken from (Chen & Papathanasiou, 2006) , each one with a porosity value equals to 0.5, δ_{min} equal to 0.1R (radious of fiber) and Nf= 196 and 900 respectively depict big flow channels as well as areas of stagnant flow. Stagnant fluid zones are common in areas where fibers have clustered together. If the gap is too small, the flow resistance can be so high that the flow channel is effectively shut. As a result, the fluid would be driven to pass through areas with less resistance.

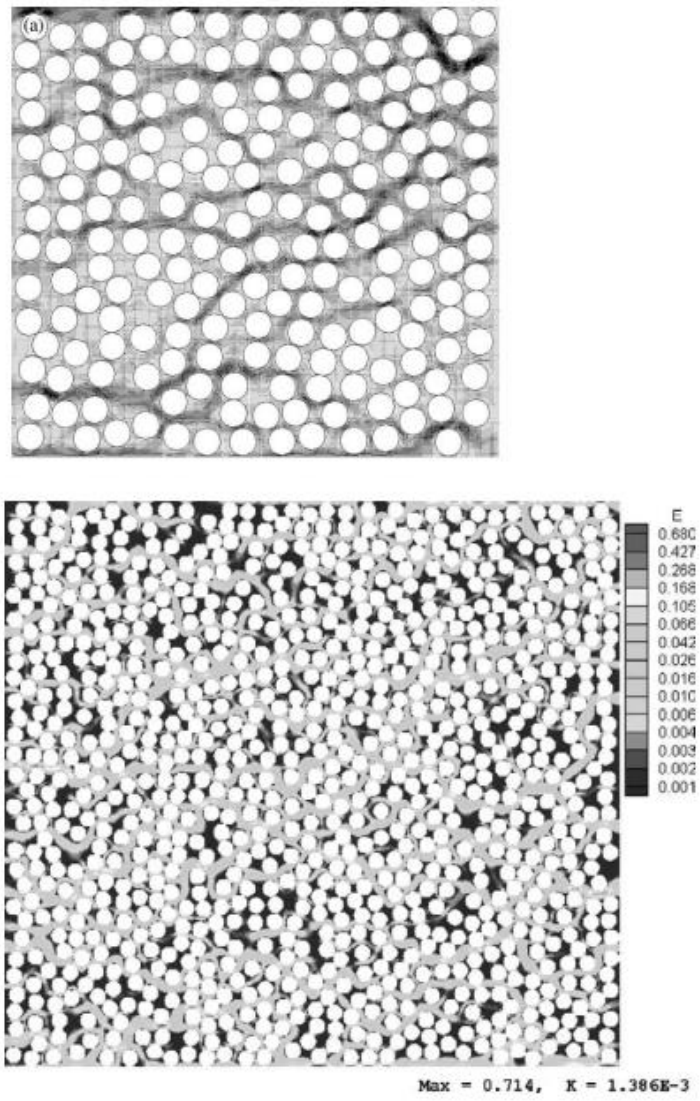

Figure 12Vector plot for a realization of random fiber array with φ=0.5, dmin=0.1R and Nf=196 (first picture) & Nf=900 (second picture). (Chen & Papathanasiou, 2006)

3.4.3.2. Kozeny Constant of fiber arrays

Generally, the permeability of a fibrous material increases as the porosity increases. A considerable dispersion in estimated permeabilities can be detected for different simulations of random fiber arrangements at the same porosity value. These dispersions suggest that using porosity alone cannot reflect the discrepancies induced by varied fiber distributions.

The Kozeny constant (kc), which appears in the Carman–Kozeny equation, has been widely utilized in the literature to highlight the dependency of permeability on the tortuosity of the porous media (Chen & Papathanasiou, 2006). To correlate with existing literature researchers transformed the permeability data into the dimensionless Kozeny constant using the following equations:

$$k_c = \frac{r_h^2}{K} * \varphi \qquad \textit{Equation 28}$$

$$r_h = \frac{D*\varphi}{4(1-\varphi)} \qquad \textit{Equation 29}$$

- r_h: mean hydraulic radius for systems of cylinders of equal size
- D: fiber diameter
- k_c: Kozeny constant (independent of porosity)

Summarizing, at low porosities, the decrease in permeability caused by increased nonuniformity in fiber arrangement. This is not surprising, since researchers have previously shown that fiber clusters can obstruct flow paths and delay flow.

This is based on the argument that reduced $<\delta_1>$ levels (mean nearest neighbor inter-fiber distance) are linked to the production of fiber bundles. Lower porosity levels followed by lower permeability (and a larger kc) and higher porosities are accompanied by the emergence of huge open areas that result in considerably higher permeability.

Non-uniformities in fiber structures are to blame for the observed permeability variances. For random fiber arrangements, the Kozeny constant is found to correlate strongly with the mean nearest neighbor inter-fiber distance $<\delta_1>$. In the examined porosity range, higher non-uniformity in fiber grids results to permeability reduction, i.e., larger values of the Kozeny constant.

3.5. PMFSS, study of the high-expectation fibrous material

One of the materials with great potential that has many applications is PMFSS, Porous Metal Fiber Sintered Sheet, a fibrous material that has the ability to be used in the development of high-performance fuel cell that is also compact in nature. This can only be done by achieving optimization in the PMFSS structural design, which in turn can only be done by evaluating the permeability of the medium, for example how the fiber structures affect the transport property (Huang et al, 2013).

This material is fairly new and is characterized by high porosity and large specific surface as well as good mechanical strength, characteristics which allow it to be successfully applied in the manufacturing of fuel cells, by using its catalytic ability for support in the gas diffusion layer. In order to prime this material and explore its full potential it became necessary to explore the correlation between transport properties of the material and pore scale morphology, in order to acquire relevant guidelines that would ultimately aid in the optimization of both performance and design (Huang et al, 2013).

3.5.1. Results of the study

As the fluid porosity increased then so did the velocity of the fluid, since it had to pass through less fibers and there was less drag force created. When the porosity was the same then the velocity of parallel flow was bigger than the velocity of the transverse flow, since alignment and direction of the fibers is a factor of permeability.

Dimensionless permeability k/r^2	Parallel Flow (x direction)	Transverse Flow (z direction)
E=90%	2.570	1.372
E=80%	0.884	0.732

Figure 13 Calculating Permeability, study results (Huang et al, 2017)

These results corroborate with the theory of the analytical model proposed by Spielman and Goren (1986), which mention that porosity and fiber arrangement significantly influence the transport property. These results are very important in the way that can be powerful tools for the optimization of the design and application of fibrous porous media by providing information on the optimal fiber arrangement and the optimal selection of flow direction.

The simulation method by Huang et al (2017) already is a tool of great importance in the construction of fiber structures and design.

3.6. Calculating Permeability of 3D isotropic and oriented fiber networks

3.6.1. The objective

When Stylianopoulos et al (2008) begun their research there wasn't a lot of work done in the field of calculating permeability in 3D random networks. A lot of factors played into that, one being that there wasn't sufficient computation power before that to calculate permeability directly via simulations.

Now, however, it is entirely possibly to directly construct entire artificial fiber networks and the flow within said networks by using a computer simulation. That can only work on small scale simulations, however, for the same reasons mentioned above: not enough computational power.

3.6.2. The method

In order to solve this problem Stylianopoulos et al (2008) developed a correlation that was based on a faction of the fiber volume, their radius and their orientation, by performing the direct calculations with a finite element method. The networks they applied them on had various degrees of orientations and combinations of parallel and perpendicular to a single fiber flow or flows perpendicular to an array of fibers and then compared their results to their analysis.

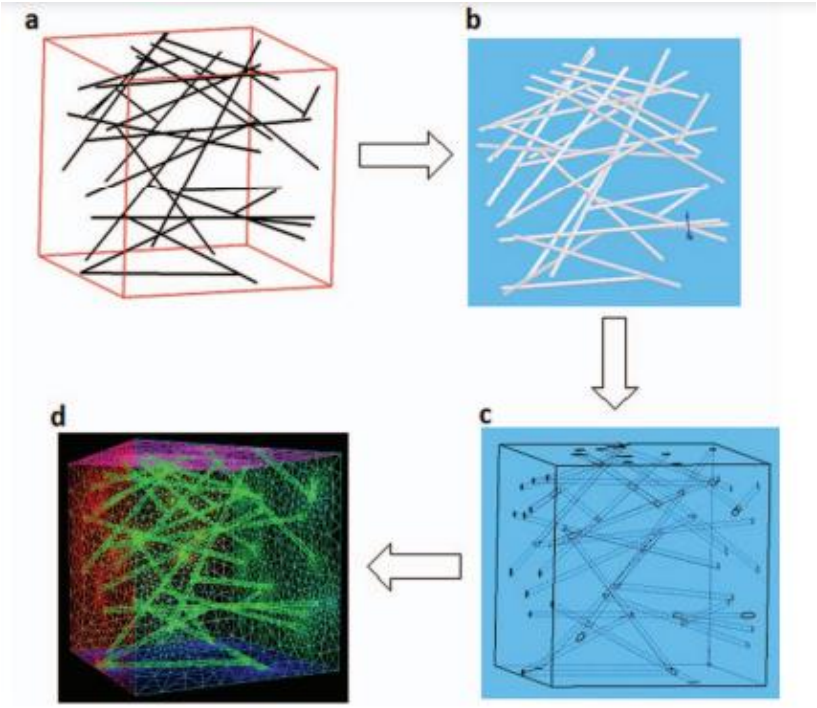

Figure 14 Generating the FE mesh from the fiber networks. Source: Stylianopoulos et al, 2008

Stylianopoulos et al (2008) generated nucleation sites at random within a cubic space and allowed them to grow in opposite directions along a random vector, growing progressively by a unit length until they reached a boundary of the network or another segment. If they reached a boundary then they generated a boundary cross-link while if they reached and collided with another segment, then they generated an interior cross-link.

The researchers used SolidWorks software to convert the fiber networks into para-solid models and created a model that depicted the fluid phase exclusively of the examined fibrous media. They imported the model into Simmetrix software and created the G- mesh, using the following conditions:

*P=Pressure and V= fluid Velocity

Stokes equation

$$\nabla P + \mu \nabla^2 V = 0 \qquad \textit{Equation 30}$$

Continuity equation

$$\nabla \cdot V = 0 \qquad \textit{Equation 31}$$

3.6.3. Results of the study

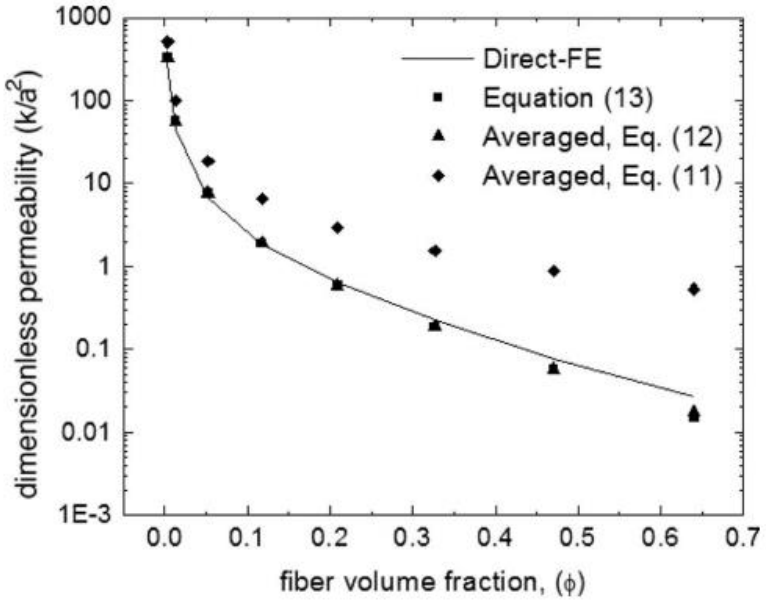

Figure 15 Calculating permeability for parallel flow. Source: Stylianopoulos et al, 2008

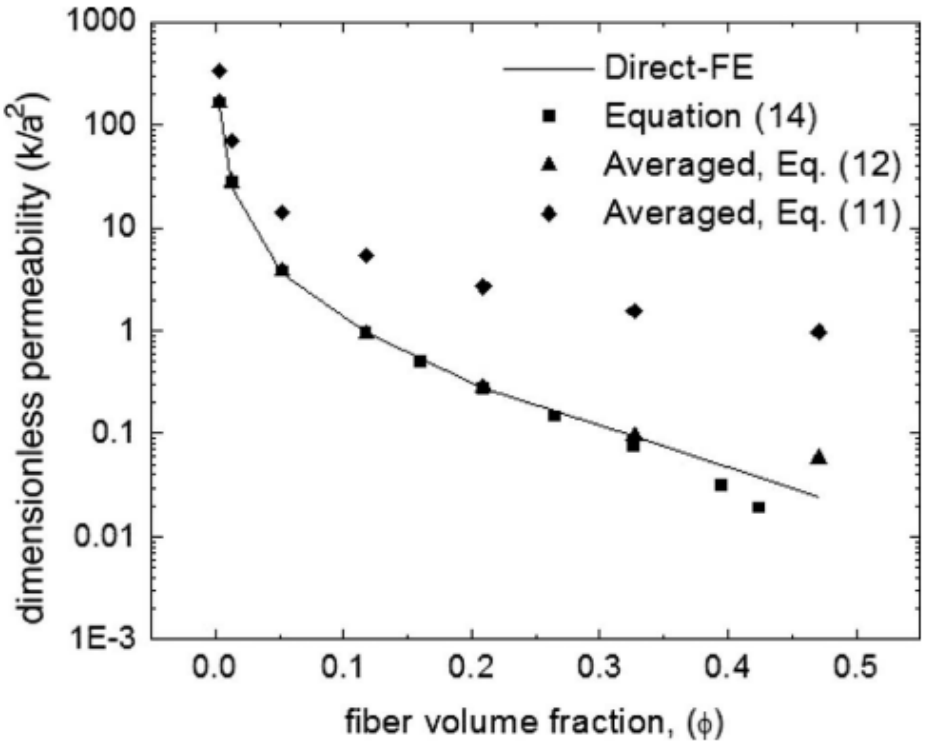

Figure 16 Calculating Permeability for transverse flow. Source: Stylianopoulos et al, 2008

Both of the figures above describe results for parallel and transverse flow for a square array of fibers. Below are the results for flows parallel and transverse to the preferred fiber direction of the moderately oriented networks (on average of five networks):

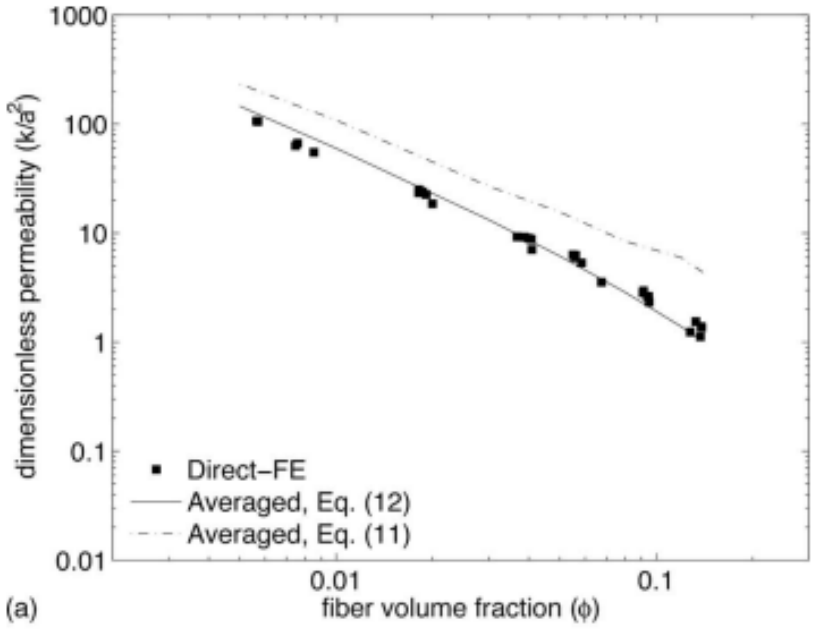

Figure 17 Permeability calculated for parallel flow to the preferred fiber direction. Source: Stylianopoulos et al, 2008

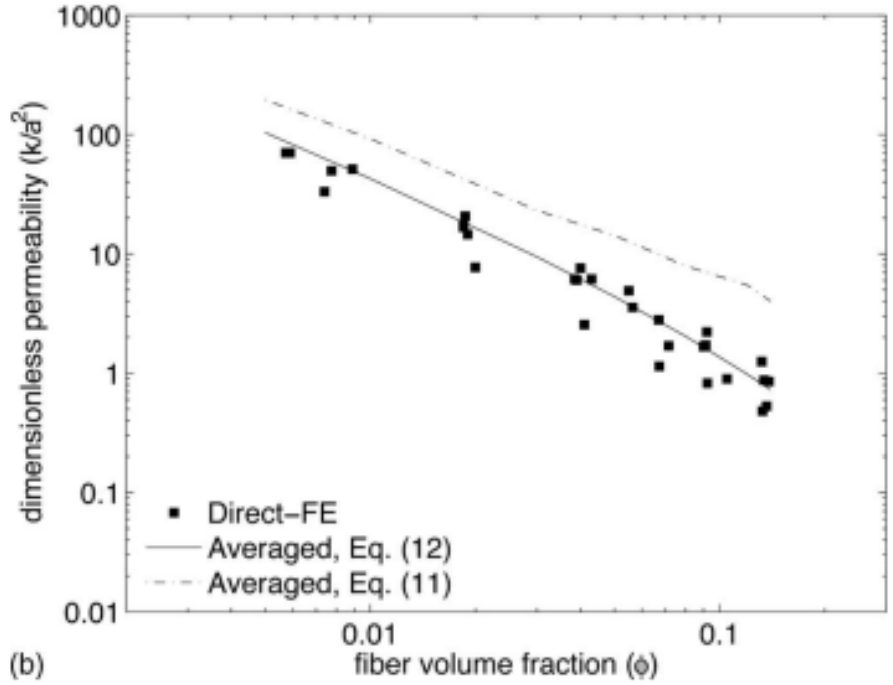

Figure 18 Permeability Calculated for flow transverse to the preferred fiber direction

The most important result of this study is that it provides the ability to explain the hydrodynamic interactions. This can be done by calculating the contribution of each fiber independently and as such provides the means to calculate permeabilities of random anisotropic networks, by knowing only the way the fibers of said network are distributed.

3.7. Summary/Conclusion

The conclusion that emerges from analyzing the studies mentioned above is that as technology evolves, people can find solutions to serious problems. We observe that the use of mathematical models, in combination with the use of tools that help simulate real fibrous materials, helps scientists to reach safe conclusions as to whether a material has high permeability due to its pores or the arrangement of its fibers.

Also, through these methods, tests can be done that will help them create such materials and use them in various areas of everyday life and industry.

Ultimately, we believe that a combination of methods rather than a single method would help scientists reach more conclusions.

Concluding, the use of artificial intelligence in this field helps us to incorporate both, features of actual fibrous media, as well as the statistical randomness, which is a key feature of such media. Also, we are able to create our own fiber bonding and study every possible case we will most likely encounter in the materials. This will help us to replace costly and time-consuming physical experiments with “virtual experiments” using computing.

CHAPTER 4

Computational Part

4.1. Computational fluids dynamics (CFD)

CFD is a methodology to solve fluid flow problems numerically. The open-source software OpenFOAM has been used as the CFD aid in the thesis. Analysis with CFD involves a number of distinct steps. First of all, the geometry must be defined and meshed, fluid properties have to be inserted and boundary conditions should be set. In the following level, the desired method of solving the problem is inserted and the arising equations solved. In the final steps, the results are pictured and computed with the help of post-processing tools such as Paraview.

4.2. First Case

4.2.1. Geometry & Mesh

4.2.1.1. GMSH Introduction

Gmsh is an open-source mesh generator evolved by Christophe Geuzaine and Jean-François Remacle. (Geuzaine & Remacle, 2009)

The Gmsh program was used to produce and generate the two-dimensional grid. Gmsh contributes to the following basic functions based on Open-Cascade Technology:

- Generating a model through geometry creation instructions.
- The discretization of a model either built in Gmsh itself or in a different program.It can make a grid in 1D, 2D and 3D models.
- The solution of differential equations on the generated discrete models.
- The ability to modify the results.

4.2.1.2. Definition of the geometry

Initially, we chose to work with Open-Cascade, and we started building our geometry, defining both the surfaces and the physical groups needed for subsequent modeling, as shown below.

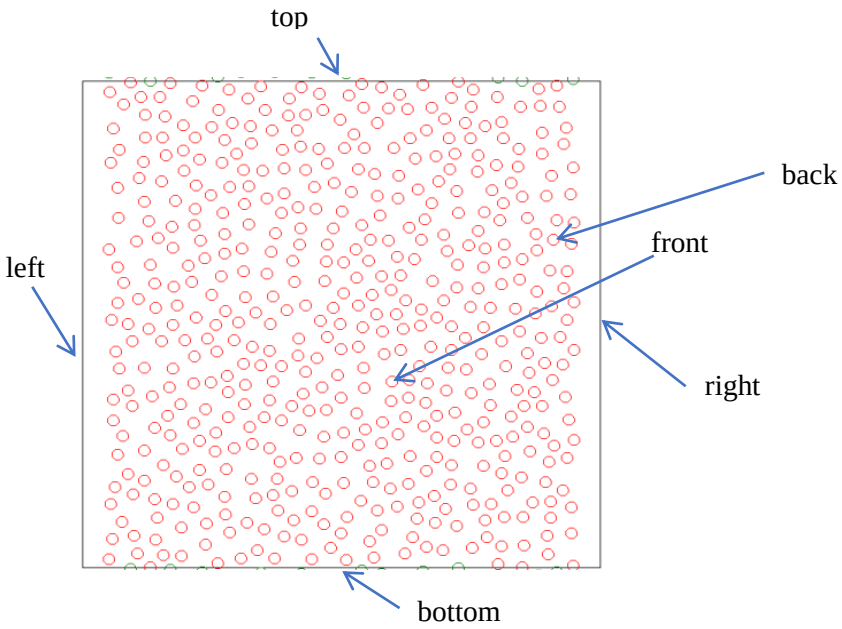

Figure 19 Fiber distribution

The geometry of our simulation was made in the Gmsh program. In particular, the grid below consists of 500 fibers with a radius of r=0.011284, volume fraction = 0.2 and a safe distance between the fibers=1.5. The length and the height of the grid is 1 cm while the depth is set to W = 0.001 (directions x, y and z in the Cartesian coordinates, respectively). Fluid flow in this geometry is considered as 2D from the left side to the right one with a velocity equal to 0.01 m/s.

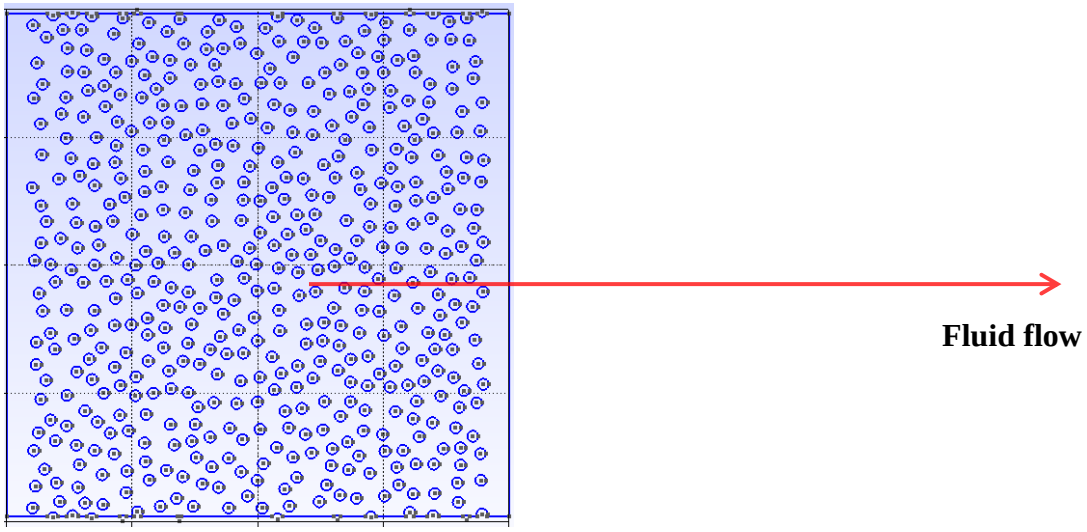

Figure 20 GMSH Geometry

In order to be able to distinguish our volume, we create a geo file with the parameters we want. More specifically, after several attempts to carry out the correct meshing, we came up with the following appropriate parameters as shown in the figure below.

```
Mesh.Algorithm = 5;
Mesh.RecombinationAlgorithm = 2;
Mesh.RecombineAll = 1;
Mesh.OptimizeNetgen = 1;
Mesh.Smoothing = 10;
Mesh.CharacteristicLengthFactor = 2.0*rd;
Mesh.CharacteristicLengthExtendFromBoundary= 0;
```

Figure 21 mesh parameters

After all the above steps have been performed and by giving the last command «Mesh 3; » we get the following final result:

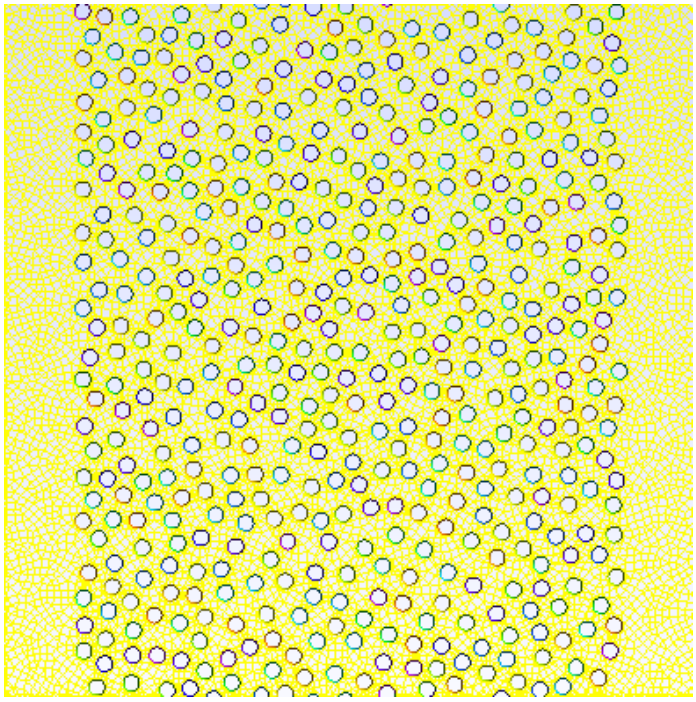

Figure 22 Final Grid

The above grid consists of 69648 nodes as well as 57312 cells and 84482 points. The statistic of the case is depicted below. Also, the mesh of the grid as well as the names of the physical groups are reflected at the below figure.

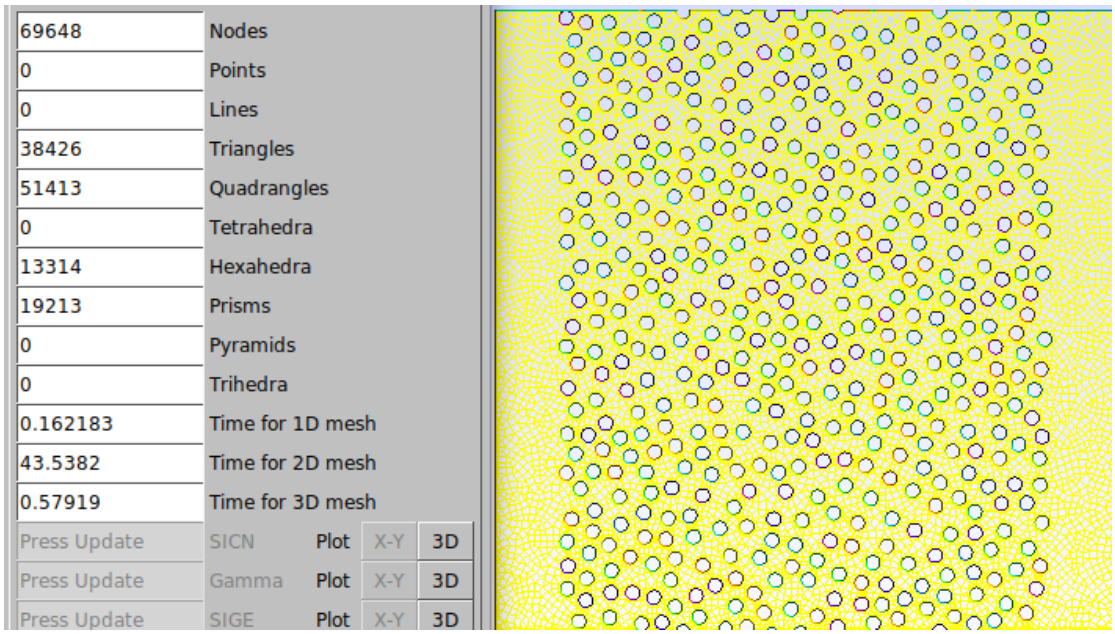

Figure 23 statistics of the geometry

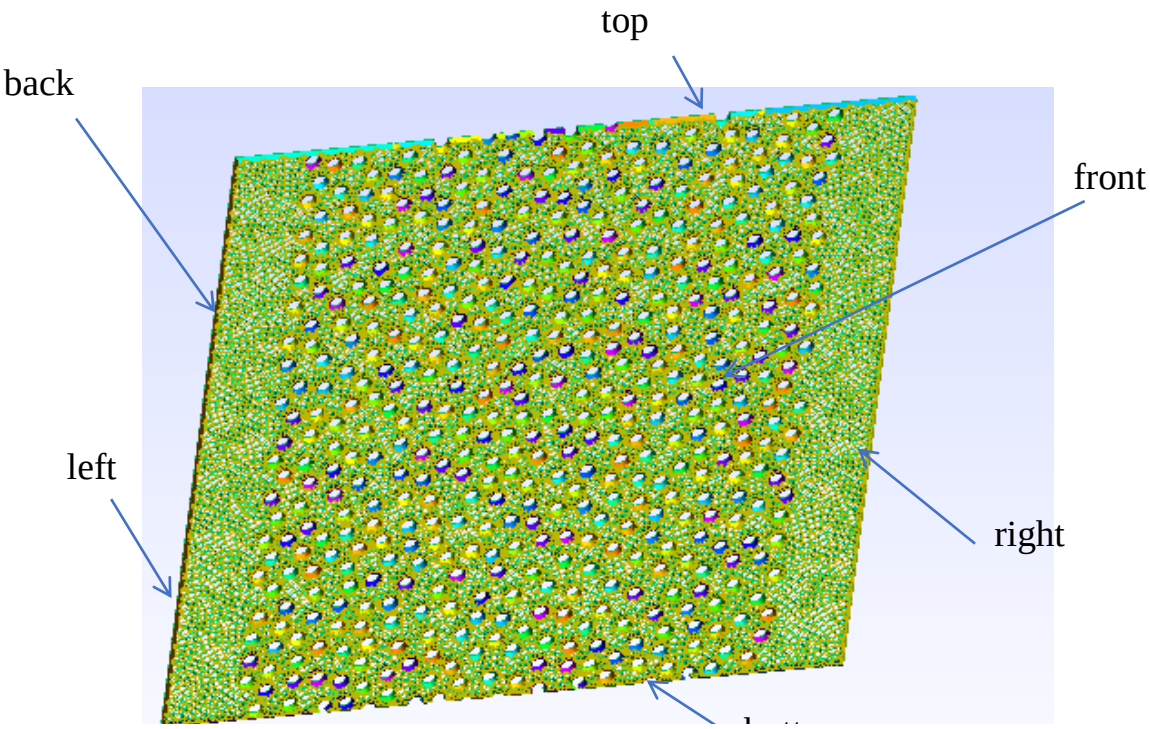

Figure 24 Final grid & physical groups

4.2.2. Case Set Up

4.2.2.1. OpenFOAM Introduction

OpenFOAM is the free, open source CFD software developed primarily by OpenCFD Ltd since 2004. It was created by Henry Weller in 1989 under the name “FOAM” and was released open source as “OpenFOAM” by Henry Weller, Chris Greenshields, and Mattijs Janssens in December 2004. (Nikolakopoulos, 2019)

OpenFOAM (“Open-source Field Operation and Manipulation”) is a C++ toolbox for the development of customized numerical solvers for fluid and continuum mechanical problems, as well as pre-/post – processing utilities for the solution of continuum mechanics problems including computational fluid dynamics (CFD). (Governance, 2012)

It is a cell-centered finite volume framework for computational fluid dynamics. OpenFoam has several tools for testing cases in many areas. The package can be used to solve many mechanical problems. As with many other CFD simulations, it includes three components, specifically, pre-processing utilities, Partial Differential Equations (PDE) solvers, and post-processing tools.

OpenFOAM is wholly programmed in C++. In combination with the fact that it is an open-source software, users are potentially able to develop additional tools for their respective needs and their demands, in order to satisfy certain specifications. Additionally, it is also relatively easy for the independently developed tools to be distributed and utilized by others with similar demands or to be developed further by other researchers. (Nikolakopoulos, 2019)

4.2.2.2. SimpleFoam Solver

OpenFOAM carries different solver approaches to best suit the different simulations. SimpleFoam is a steady state solver used to test the motion of incompressible flows.

The equations that demonstrate the behavior of a fluid are non-linear differential equations. These equations are used in Newtonian fluids. There are three equations, the continuity equation (32) that depicts the conservation of mass, the momentum or Navier-Stokes equation (33) which constitutes the second law of Newton depending on a fluid and include the relation between pressure and velocity. Finally, the energy equation (34) that presents the heat transference in the fluid. The equations are depicted below:

$$\frac{\partial \rho}{\partial t} + \nabla \cdot (\rho \boldsymbol{u}) = 0 \qquad \textit{Equation 32}$$

$$\frac{\partial (\rho u)}{\partial t} + \rho \boldsymbol{u} \cdot \nabla(\boldsymbol{u}) = -\nabla p + \rho \boldsymbol{g} + \nabla \cdot \boldsymbol{\tau} \qquad \textit{Equation 33}$$

$$\rho c \frac{\partial T}{\partial t} + \rho c \boldsymbol{u} \cdot \nabla(T) = \nabla \cdot (\kappa \nabla T) + \Phi \qquad \textit{Equation 34}$$

P is the density of the fluid, t is the temporal variable, p represents the pressure, g depicts the acceleration of gravity, τ is the shear-stress tensor, κ is the conductivity of the fluid, T the temperature, c the specific heat capacity and Φ expresses the energetic dissipation.

Due to the incompressibility, the energy equation (34) does not need to be solved, because there is no connection between the momentum and continuity equations. Instead, the momentum equation is solved, and a pressure adjustment is executed, thus a physical pressure is not solved but rather pressure differences are found. (Winter, 2013)

The first equation (32) presents that the divergence of the velocity may be zero, that means that the fluid can't expand (positive divergence) nor compress (negative divergence).

The second equation (33), the momentum equation, presents the connection between the velocity, pressure, and outer forces of the incompressible fluid.

4.2.2.2. Fluid Properties

In addition to the acceptances used to extract these equations, the below assumptions are made for this Thesis:

1. Steady state conditions due to constant density and viscosity ($\partial / \partial t = 0$)

2. Incompressible flow (Mach number < 0.3)

3. 2D flow

4. Laminar flow (Re<2300)

For our viscosity model we used a Newtonian fluid (for example, water).

Therefore, we set:

- Kinematic Viscosity: $v = 10^{-6}\ m^2/s^2$
- Dynamic viscosity: $\mu = 1.19 * 10^{-3}\ kg/m*s$
- Density: $\rho = 1\ kg/m^3$

The Reynolds number for our case is computed equal to 225, which confirms our assumption for laminar flow.

$$Re = \frac{\rho u D}{\mu} = \frac{u D}{\nu} = \frac{0.01 * 0.02256}{1e-6} = 225 \qquad \textit{Equation 35}$$

4.2.2.3. Boundary Conditions

The below figure presents the exact case which is simulated with OpenFOAM in parallel.

In brief, the 0 folder constitutes the boundary conditions of the parameters at all the boundaries in the mesh along with the elementary values of the parameters mentioned under the ”0” subfolder at time 0. The constant folder contains a description of the case mesh in subdirectory polyMesh and files specifying physical properties for the application concerning the transport properties and momentumTransport files. Finally, the system folder is for setting parameters associated with the solution procedure itself. It contains at least 3 files controlDict, fvSchemes and fvSolution in which time stepping, discretization schemes and linear solvers are stated. (Prakash Reddy Samala et al,2015)

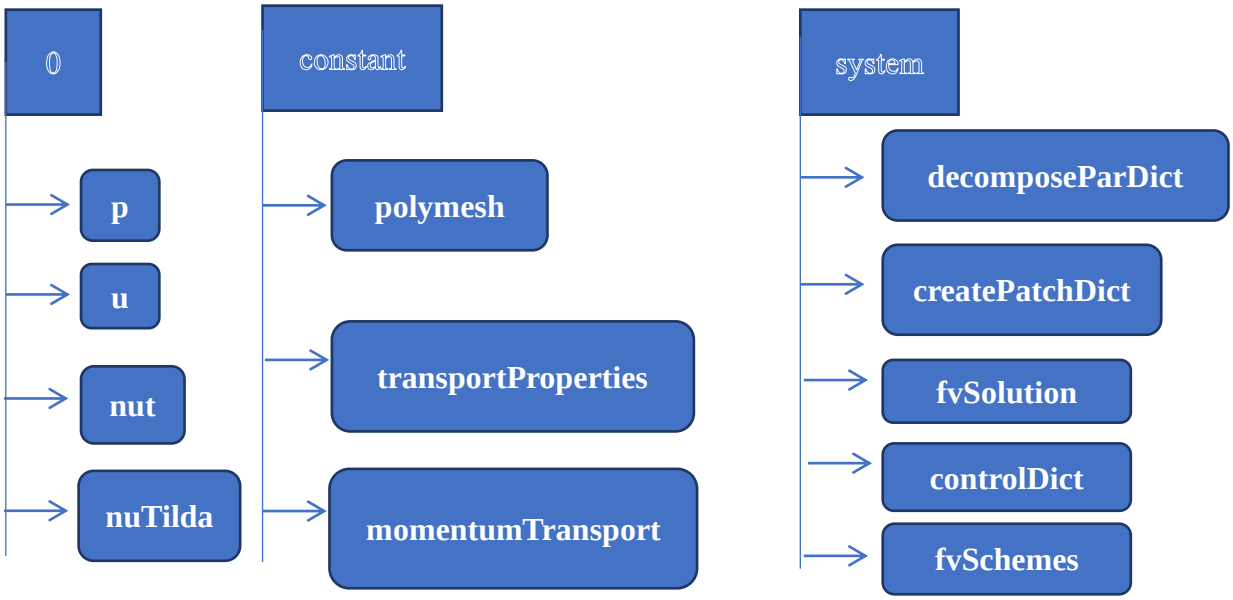

Figure 25 Openfoam case set-up

In the next subsection, some functions of each subfolder and snapshots of the case solved will be presented in detail.

0 FOLDER

The 0 folder as shown in the above flow chart includes the files to specify boundary conditions and initial values for pressure (p) and velocity (U) which are usual for any case that should be tested. The other parameters range depending on the turbulence model.

For laminar, incompressible flow, only files including the boundary conditions of U and p are required. For turbulence models other variables will be required as well.

The dimension of the variable is allocated through dimensions in the folder (for instance m/s for the velocity). The internal field is set through internalField and the boundary field is given through boundaryField.

```
/*--------------------------------*- C++ -*----------------------------------*\
  =========                 |
  \\      /  F ield         | OpenFOAM: The Open Source CFD Toolbox
   \\    /   O peration     | Website:  https://openfoam.org
    \\  /    A nd           | Version:  8
     \\/     M anipulation  |
\*---------------------------------------------------------------------------*/
FoamFile
{
    version     2.0;
    format      ascii;
    class       volScalarField;
    object      nuTilda;
}
// * * * * * * * * * * * * * * * * * * * * * * * * * * * * * * * * * * * * //

dimensions      [0 2 -1 0 0 0 0];

internalField   uniform 0.14;

boundaryField
{
    left
    {
        type            freestream;
        freestreamValue uniform 0.14;
    }

    right
    {
        type            freestream;
        freestreamValue uniform 0.14;
    }

    top
    {
        type            fixedValue;
        value           uniform 0;
    }
    bottom
    {
        type            fixedValue;
        value           uniform 0;
    }

    front
    {
        type            empty;
    }

    back
    {
        type            empty;
    }

    cylinder
    {
        type            fixedValue;
        value           uniform 0;
    }
}

// ************************************************************************* //
```

```
/*--------------------------------*- C++ -*----------------------------------*\
  =========                 |
  \\      /  F ield         | OpenFOAM: The Open Source CFD Toolbox
   \\    /   O peration     | Website:  https://openfoam.org
    \\  /    A nd           | Version:  8
     \\/     M anipulation  |
\*---------------------------------------------------------------------------*/
FoamFile
{
    version     2.0;
    format      ascii;
    class       volScalarField;
    object      nut;
}
// * * * * * * * * * * * * * * * * * * * * * * * * * * * * * * * * * * * * //

dimensions      [0 2 -1 0 0 0 0];

internalField   uniform 0.14;

boundaryField
{
    left
    {
        type            freestream;
        freestreamValue uniform 0.14;
    }

    right
    {
        type            freestream;
        freestreamValue uniform 0.14;
    }

    bottom
    {
        type            nutUSpaldingWallFunction;
        value           uniform 0;
    }
    top
    {
        type            nutUSpaldingWallFunction;
        value           uniform 0;
    }

    front
    {
        type            empty;
    }

    back
    {
        type            empty;
    }
    cylinder
    {
        type            nutUSpaldingWallFunction;
        value           uniform 0;
    }
}

// ************************************************************************* //
```

Figure 26 nuTilda & nut subFolders

```
/*--------------------------------*- C++ -*----------------------------------*\
  =========                 |
  \\      /  F ield         | OpenFOAM: The Open Source CFD Toolbox
   \\    /   O peration     | Website:  https://openfoam.org
    \\  /    A nd           | Version:  8
     \\/     M anipulation  |
\*---------------------------------------------------------------------------*/
FoamFile
{
    version     2.0;
    format      ascii;
    class       volVectorField;
    object      U;
}
// * * * * * * * * * * * * * * * * * * * * * * * * * * * * * * * * * * * * //

dimensions      [0 1 -1 0 0 0 0];

internalField   uniform (0 0 0);

boundaryField
{
    left
    {
        type fixedValue;
        value uniform (0.01 0 0);
    }

    right
    {
     type zeroGradient;
    }

    top
    {
       type  fixedValue;
       value uniform (0 0 0);
    }

   bottom
    {
       type  fixedValue;
       value uniform (0 0 0);
    }

    front
    {
        type    empty;
    }
    back
    {
        type empty;
    }
    cylinder //san wall
    {
        type  fixedValue;
        value uniform (0 0 0);
    }
}

// ************************************************************************* //
```

```
/*--------------------------------*- C++ -*----------------------------------*\
  =========                 |
  \\      /  F ield         | OpenFOAM: The Open Source CFD Toolbox
   \\    /   O peration     | Website:  https://openfoam.org
    \\  /    A nd           | Version:  8
     \\/     M anipulation  |
\*---------------------------------------------------------------------------*/
FoamFile
{
    version     2.0;
    format      ascii;
    class       volScalarField;
    object      p;
}
// * * * * * * * * * * * * * * * * * * * * * * * * * * * * * * * * * * * * //

dimensions      [0 2 -2 0 0 0 0];

internalField   uniform 0;

boundaryField
{
    left
     {
    type zeroGradient;
    }

    right
    {
      type fixedValue;
      value uniform 1;
    }

    front
    {
        type empty;
    }

        back
    {
        type empty;
    }

    top
    {
       type zeroGradient;
        }

    bottom
    {
        type zeroGradient;
        }

        cylinder
        {
    type zeroGradient;
        }
}

// ************************************************************************* //
```

Figure 27 u & p subFolders

SYSTEM FOLDER

This folder contains the specifications for the simulation. (Winter, 2013)

- In the decomposeParDict file the mesh is decomposed into an assigned number of parts for parallel simulations and the user can specify which decomposition technique will be used and how many processing nodes the mesh will be divided on. (Winter, 2013)

- The schemes file allows users to select appropriate discretization schemes

- The fvSolution file contains the linear solvers for the sequential equations are assigned. Also the linear solver tolerance and maximum number of iterations are assigned here. (Winter, 2013)

- The controlDict file contains time settings to store to the mesh calculated.

```
/*--------------------------------*- C++ -*----------------------------------*\
  =========                 |
  \\      /  F ield         | OpenFOAM: The Open Source CFD Toolbox
   \\    /   O peration     | Website:  https://openfoam.org
    \\  /    A nd           | Version:  8
     \\/     M anipulation  |
\*---------------------------------------------------------------------------*/
FoamFile
{
    version     2.0;
    format      ascii;
    class       dictionary;
    location    "system";
    object      fvSolution;
}
// * * * * * * * * * * * * * * * * * * * * * * * * * * * * * * * * * * * * //

solvers
{
    p
    {
        solver          GAMG;
        tolerance       1e-06;
        relTol          0.1;
        smoother        GaussSeidel;
    }

    U
    {
        solver          smoothSolver;
        smoother        GaussSeidel;
        nSweeps         2;
        tolerance       1e-08;
        relTol          0.1;
    }

    nuTilda
    {
        solver          smoothSolver;
        smoother        GaussSeidel;
        nSweeps         2;
        tolerance       1e-08;
        relTol          0.1;
    }
}

SIMPLE
{
    nNonOrthogonalCorrectors 4;

    residualControl
    {
        p               1e-5;
        U               1e-5;
        nuTilda         1e-5;
    }
}

relaxationFactors
{
    fields
    {
        p               0.3;
    }
    equations
    {
        U               0.7;
        nuTilda         0.7;
    }
}
```

```
/*--------------------------------*- C++ -*----------------------------------*\
| =========                 |                                                 |
| \\      /  F ield         | OpenFOAM: The Open Source CFD Toolbox           |
|  \\    /   O peration     | Version:  2.4.0                                 |
|   \\  /    A nd           | Web:      www.OpenFOAM.org                      |
|    \\/     M anipulation  |                                                 |
\*---------------------------------------------------------------------------*/
FoamFile
{
    version     2.0;
    format      ascii;
    class       dictionary;
    location    "system";
    object      decomposeParDict;
}
// * * * * * * * * * * * * * * * * * * * * * * * * * * * * * * * * * * * * //

numberOfSubdomains 4;

method          scotch;

simpleCoeffs
{
    n   (4 1 1);
    delta           0.001;
}

scotchCoeffs
{
        processorWeights ( 1 1 1 1 );

}

hierarchicalCoeffs
{
    n               ( 1 1 1 );
    delta           0.001;
    order           xyz;
}

manualCoeffs
{
    dataFile        "";
}

distributed     no;

roots           ( );
```

Figure 28 fvSolution & decomposeParDict subFolders

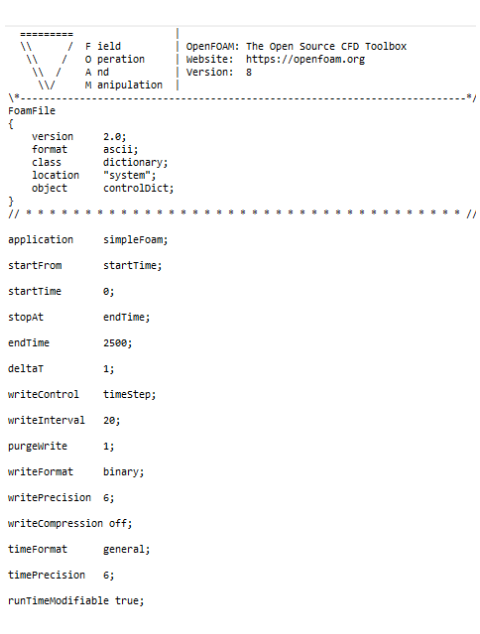

```
  =========                 |
  \\      /  F ield         | OpenFOAM: The Open Source CFD Toolbox
   \\    /   O peration     | Website:  https://openfoam.org
    \\  /    A nd           | Version:  8
     \\/     M anipulation  |
\*---------------------------------------------------------------------------*/
FoamFile
{
    version     2.0;
    format      ascii;
    class       dictionary;
    location    "system";
    object      controlDict;
}
// * * * * * * * * * * * * * * * * * * * * * * * * * * * * * * * * * * * * //

application     simpleFoam;

startFrom       startTime;

startTime       0;

stopAt          endTime;

endTime         2500;

deltaT          1;

writeControl    timeStep;

writeInterval   20;

purgeWrite      1;

writeFormat     binary;

writePrecision  6;

writeCompression off;

timeFormat      general;

timePrecision   6;

runTimeModifiable true;

// ************************************************************************* //
```

```
/*--------------------------------*- C++ -*----------------------------------*\
  =========                 |
  \\      /  F ield         | OpenFOAM: The Open Source CFD Toolbox
   \\    /   O peration     | Website:  https://openfoam.org
    \\  /    A nd           | Version:  8
     \\/     M anipulation  |
\*---------------------------------------------------------------------------*/
FoamFile
{
    version     2.0;
    format      ascii;
    class       dictionary;
    location    "system";
    object      fvSchemes;
}
// * * * * * * * * * * * * * * * * * * * * * * * * * * * * * * * * * * * * //

ddtSchemes
{
    default         steadyState;
}

gradSchemes
{
    default         Gauss linear;
}

divSchemes
{
    default         none;
    div(phi,U)      bounded Gauss linearUpwind grad(U);
    div(phi,nuTilda) bounded Gauss linearUpwind grad(nuTilda);
    div((nuEff*dev2(T(grad(U))))) Gauss linear;
}

laplacianSchemes
{
    default         Gauss linear corrected;
}

interpolationSchemes
{
    default         linear;
}

snGradSchemes
{
    default         corrected;
}

wallDist
{
    method meshWave;
}

// ************************************************************************* //
```

Figure 29 controlDict & fvSchemes subFolders

CONSTANT FOLDER

This folder includes specifications for turbulence and fluid properties. Depending on the solver chosen, different files need to be described.

- The kind of turbulence model required is established in turbulenceProperties where either LES, RAS or laminar model can be selected.

- For incompressible solvers the file transportProperties establishes the behavior of the kinematic viscosity v.

OpenFOAM uses a cell-centered control volume for its calculations. In the polyMesh folder files are contained describing the mesh. These files include points, which contain the points of the mesh, faces, which contain the faces of the cells, owner, that contains what faces belong to a cell and neighbour which contains the information about the connectivity between cells. (Winter, 2013)

```
/*--------------------------------*- C++ -*----------------------------------*
  =========                 |
  \\      /  F ield         | OpenFOAM: The Open Source CFD Toolbox
   \\    /   O peration     | Website:  https://openfoam.org
    \\  /    A nd           | Version:  8
     \\/     M anipulation  |
\*---------------------------------------------------------------------------*
FoamFile
{
    version     2.0;
    format      ascii;
    class       dictionary;
    location    "constant";
    object      momentumTransport;
}
// * * * * * * * * * * * * * * * * * * * * * * * * * * * * * * * * * * * * * /

simulationType laminar;

RAS
{
    model           kepsilon;

    turbulence      off;

    printCoeffs     on;
}

// ************************************************************************* /
```

```
/*--------------------------------*- C++ -*----------------------------------*\
  =========                 |
  \\      /  F ield         | OpenFOAM: The Open Source CFD Toolbox
   \\    /   O peration     | Website:  https://openfoam.org
    \\  /    A nd           | Version:  8
     \\/     M anipulation  |
\*---------------------------------------------------------------------------*/
FoamFile
{
    version     2.0;
    format      ascii;
    class       dictionary;
    location    "constant";
    object      transportProperties;
}
// * * * * * * * * * * * * * * * * * * * * * * * * * * * * * * * * * * * * * //

transportModel  Newtonian;

nu              [0 2 -1 0 0 0 0] 1e-06;

// ************************************************************************* //
```

Figure 30 momentumTransport&transportProperties subfolders

4.2.3. Results

4.2.3.1. Simplefoam

After the simulation, OpenFoam calculates the value of the flow rate (Q) which is equal, for our case, to the value of Q= 9.9995*10^{-9} m^3/s.

Also, the value of the average patch area is A = 0.01(y) *0.0001(z) =10^{-6} m^2.

Finally, the average value of the velocity is calculated by the following equation:

$$uavg = \frac{Q}{A} = 9.9995 * 10^{-3}\ m/s \qquad \textit{Equation 36}$$

The number of Reynolds once again confirms the choice of simplefoam as the most appropriate choice because:

$$Re = \frac{uavg * Dfiber}{v} = 225 \quad \textit{(Laminar flow)} \qquad \textit{Equation 37}$$

- U_{avg} = 9.9995 *10^{-3} m/s
- D_{fiber}= 0.02256 m
- V=10^{-6} m^2/s^2

4.2.3.2. Paraview

ParaView is an open-source application used for post-processing and visualizing the results from the calculations made by OpenFOAM. It is a multi-platform data analysis made by Kitware Inc. and is free to download for any user. The software is very adaptable, being able to run on any of the modern operating systems as well as on any computer system ranging from smaller personal computers to larger super computers analyzing extremely large datasets. (Sihvo, 2014)

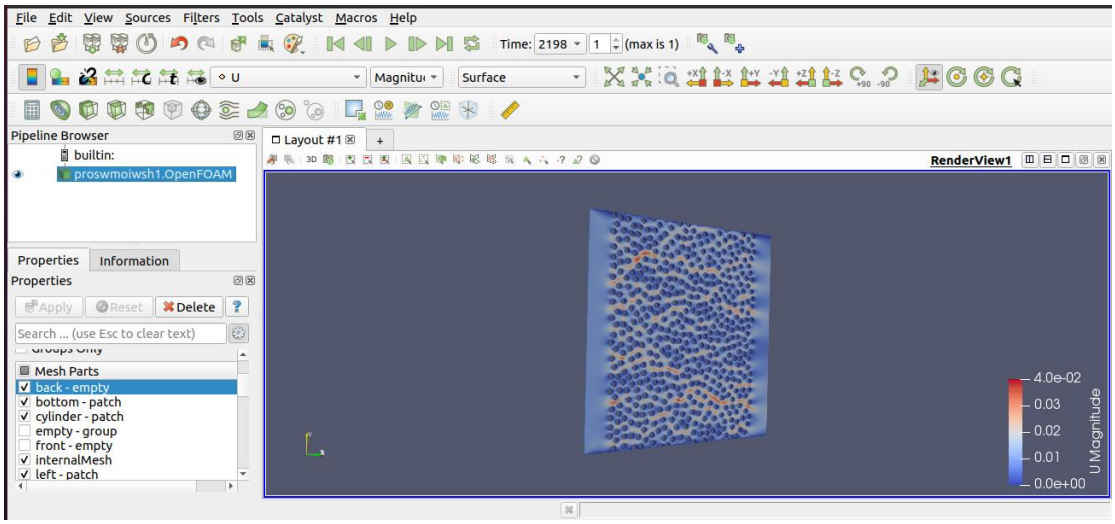

Figure 31 workbench of paraview 5.6.0

The above figure shows the workbench of ParaView 5.6.0 that was used for post processing for this thesis work.

When the chosen solver has come to the maximum time steps and the case has been recreated, the case files and results can be seen in the software ParaView or any other post-processing application.

A sample of how the results can be viewed is seen in the below figures which depict the velocity profile at the end of the grid.

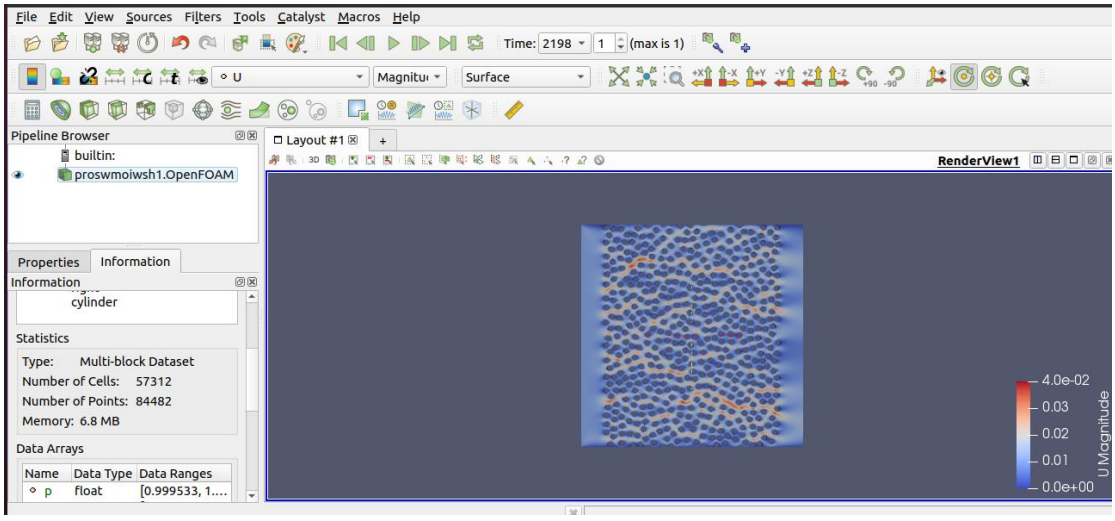

Figure 32 Velocity Profile (1)

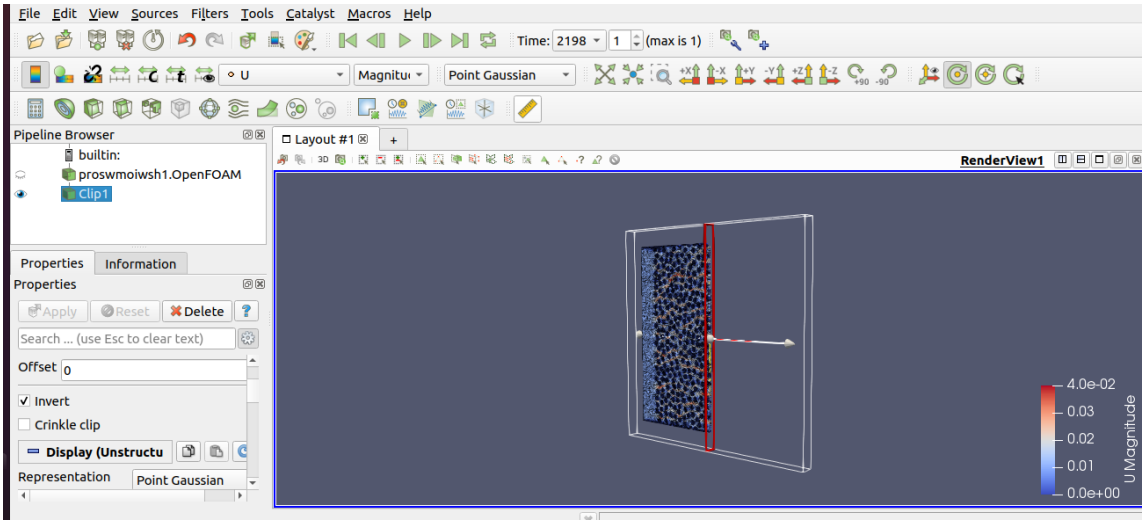

Figure 33 velocity profile (2)

4.2.4. Residence Time Distribution (RTD)

The residence time distribution (RTD) is a probability distribution function that describes the time a particle could spend inside the grid. The residence time distribution (RTD) function, introduced firstly by Danckwerts in 1953, is a useful tool to investigate the time a material spends inside a grid. (Verclyte, 2012)

The distribution of residence times is represented by an exit age distribution, E(t), and a cumulative residence time distribution function, F(t). The area under the curve of the graph of tracer concentration against time is normalized by dividing the concentration values by the total area under the curve, thus giving the E(t) values. (Verclyte, 2012)

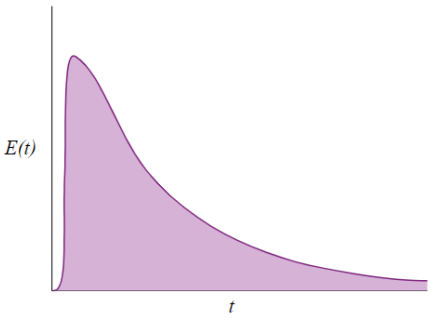

Figure 34 RTD Diagram, (Tutorial Ten Residence Time Distribution, 2018)

$$E(t) = \frac{C(t)}{\int_0^\infty C(t)dt} = \frac{tracer\ concentration\ at\ time\ t}{Total\ tracer\ concentration} \qquad \textbf{Equation 38}$$

Since all tracer elements will leave the grid at some point, RTD satisfies the following relationship: (*Tutorial Ten Residence Time Distribution*, 2018)

$$F(t) = \int_0^\infty E(t)dt = 1 \qquad \textit{Equation 39}$$

The Residence Time Distribution (RTD) is derived from placing an inert tracer into the system at t = 0 and calculating the tracer concentration in the outlet. The particle should not react. The physical properties of the tracer may be similar to the ones of the fluid, and it should not influence the flow behavior of the fluid in the system.

The tracers are small particles with density equal to 1 kg/m^3 (similar to fluid's density) and in simulations are depicted as colored materials.

In a continuous laminar flow system, an RTD function can be used only if the velocity distribution in the grid is known and there is enough knowledge to predict the flow of every fluid tracer.

4.2.4.1. ScalarTransportFoam Solver

As in the (Horvat, 2016) is presented, Scalar transport equation models a combination of convection and diffusion transport of scalar. Equation in standard form can analytically be expressed as:

$$\frac{\partial T}{\partial t} + \nabla \cdot (uT) - \nabla \cdot (D\tau \nabla T) = qv \qquad \textit{Equation 40}$$

Where T is the transported scalar variable, u is the convective velocity and Dτ is the diffusion coefficient.

The term on right hand side of Eq. (40) represents sources or sinks of the transported scalar T. Sources and sinks account for non-transport effects such as local volume production and destruction of T. (Horvat, 2016)

In standard form of scalar transport equation four characteristic terms are presented: • term $\frac{\partial T}{\partial t}$ is the temporal derivative of transported scalar which represents inertia of the system, • term ∇·(uT) is the convection term which represents the convective transport of scalar T by the velocity field u, •term ∇·(Dτ∇T) is the diffusion term which represents transport of scalar T based on its spatial gradient and diffusivity Dτ, • term qv represents sources and sinks of transported scalar T. (Horvat, 2016)

The scalarTransportFoam solver determines a convection-diffusion scalar transport equation without source terms. As a result, eq.40 can be expressed as:

$$\frac{\partial T}{\partial t} + \nabla \cdot (uT) - \nabla \cdot (D\tau \nabla T) = 0 \qquad \textit{Equation 41}$$

4.2.4.2. Boundary Conditions

Simulations were executed using the scalarTransportFoam solver. This is used to visualize the distribution of the tracer concentration throughout the system.

In order to accomplish the scalarTransportFoam simulation, the velocity folder is copied from the last step of the simpleFoam simulation, in to the "u/0 "subfolder of the scalarTransportFoam simulation case.

The below figure constitutes the exact case which is simulated with OpenFOAM in parallel.

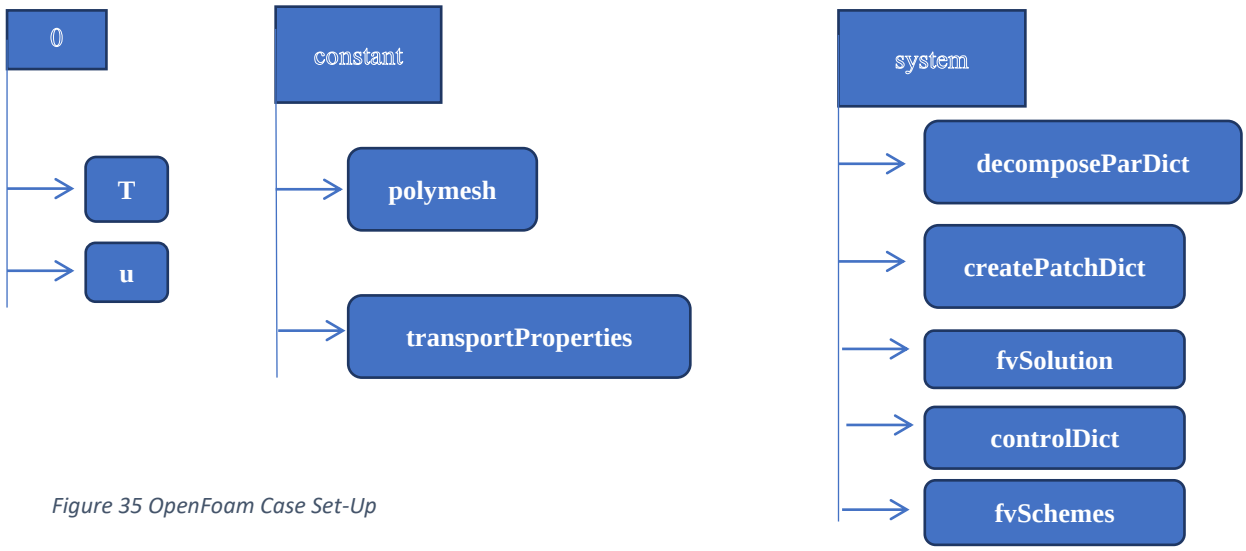

Figure 35 OpenFoam Case Set-Up

0 FOLDER

As we already explained at the description of the simplefoam solver, and for scalarTransportFoam, the"0" file includes two files namely one for the velocity field and the other for the concentration/scalar field. But the initial and boundary conditions were determined only for the scalar field while the velocity file is copied from the simpleFoam case at the simulation latest time, as we already said. (Mekonnen, 2016.)

```
/*--------------------------------*- C++ -*----------------------------------*\
  =========                 |
  \\      /  F ield         | OpenFOAM: The Open Source CFD Toolbox
   \\    /   O peration     | Website:  https://openfoam.org
    \\  /    A nd           | Version:  8
     \\/     M anipulation  |
\*---------------------------------------------------------------------------*/
FoamFile
{
    version     2.0;
    format      ascii;
    class       volScalarField;
    object      T;
}
// * * * * * * * * * * * * * * * * * * * * * * * * * * * * * * * * * * * * //

dimensions      [0 0 0 1 0 0 0];

internalField   uniform 0;

boundaryField
{
    left
    {
        type            fixedValue;
        value           uniform 1;
    }

    right
    {
        type            zeroGradient;
    }

    top
    {
        type            zeroGradient;
    }
    bottom
    {
        type            zeroGradient;
    }
    cylinder
    {
        type            zeroGradient;
    }
    front
    {
        type            empty;
    }
    back
    {
        type            empty;
    }
}
// ************************************************************************* //
```

Figure 36 T SubFolder

CONSTANT FOLDER

For the scalarTransportFoam case, the only asset that must be defined is the diffusion coefficient of the tracer which is saved in the transportProperties dictionary.

```
/*--------------------------------*- C++ -*----------------------------------*\
  =========                 |
  \\      /  F ield         | OpenFOAM: The Open Source CFD Toolbox
   \\    /   O peration     | Website:  https://openfoam.org
    \\  /    A nd           | Version:  8
     \\/     M anipulation  |
\*---------------------------------------------------------------------------*/
FoamFile
{
    version     2.0;
    format      ascii;
    class       dictionary;
    location    "constant";
    object      transportProperties;
}
// * * * * * * * * * * * * * * * * * * * * * * * * * * * * * * * * * * * * //

DT              DT [0 2 -1 0 0 0 0] 0.01;


// ************************************************************************* //
```

Figure 37 TransportProperties

SYSTEM FOLDER

This folder contains the details for the simulation. The functions of each subfolder remain the same as presented in detail at a previous section.

```
/*--------------------------------*- C++ -*----------------------------------*\
| =========                 |                                                 |
| \\      /  F ield         | OpenFOAM: The Open Source CFD Toolbox           |
| \\    /   O peration     | Version:  2.4.0                                 |
|  \\  /    A nd           | Web:      www.OpenFOAM.org                      |
|   \\/     M anipulation  |                                                 |
\*---------------------------------------------------------------------------*/
FoamFile
{
    version     2.0;
    format      ascii;
    class       dictionary;
    location    "system";
    object      decomposeParDict;
}
// * * * * * * * * * * * * * * * * * * * * * * * * * * * * * * * * * * * * //

numberOfSubdomains 4;

method          scotch;

simpleCoeffs
{
    n   (4 1 1);
    delta           0.001;
}

scotchCoeffs
{
       processorWeights ( 1 1 1 1 );

}

hierarchicalCoeffs
{
    n               ( 1 1 1 );
    delta           0.001;
    order           xyz;
}

manualCoeffs
{
    dataFile        "";
}

distributed     no;

roots           ( );

// ************************************************************************* //
```

Figure 38 DecomposeParDict

```
/*--------------------------------*- C++ -*----------------------------------*\
  =========                 |
  \\      /  F ield         | OpenFOAM: The Open Source CFD Toolbox
   \\    /   O peration     | Website:  https://openfoam.org
    \\  /    A nd           | Version:  8
     \\/     M anipulation  |
\*---------------------------------------------------------------------------*/
FoamFile
{
    version     2.0;
    format      ascii;
    class       dictionary;
    location    "system";
    object      controlDict;
}
// * * * * * * * * * * * * * * * * * * * * * * * * * * * * * * * * * * * * //

application     scalarTransportFoam;

startFrom       startTime;

startTime       0;

stopAt          endTime;

endTime         0.065;

deltaT          0.0005;

writeControl    timeStep;

writeInterval   1;

purgeWrite      0;

writeFormat     binary;

writePrecision  6;

writeCompression off;

timeFormat      general;

timePrecision   6;

runTimeModifiable true;

// ************************************************************************* //
```

Figure 39 controlDict

```
/*--------------------------------*- C++ -*----------------------------------*\
  =========                 |
  \\      /  F ield         | OpenFOAM: The Open Source CFD Toolbox
   \\    /   O peration     | Website:  https://openfoam.org
    \\  /    A nd           | Version:  8
     \\/     M anipulation  |
\*---------------------------------------------------------------------------*/
FoamFile
{
    version     2.0;
    format      ascii;
    class       dictionary;
    location    "system";
    object      fvSolution;
}
// * * * * * * * * * * * * * * * * * * * * * * * * * * * * * * * * * * * * //

solvers
{
    T
    {
        solver          PBiCGStab;
        preconditioner  DILU;
        tolerance       1e-06;
        relTol          0;
    }
}

SIMPLE
{
    nNonOrthogonalCorrectors 0;
}


// ************************************************************************* //
```

Figure 40 fvSlution

```
/*--------------------------------*- C++ -*----------------------------------*\
  =========                 |
  \\      /  F ield         | OpenFOAM: The Open Source CFD Toolbox
   \\    /   O peration     | Website:  https://openfoam.org
    \\  /    A nd           | Version:  8
     \\/     M anipulation  |
\*---------------------------------------------------------------------------*/
FoamFile
{
    version     2.0;
    format      ascii;
    class       dictionary;
    location    "system";
    object      fvSchemes;
}
// * * * * * * * * * * * * * * * * * * * * * * * * * * * * * * * * * * * * //

ddtSchemes
{
    default         Euler;
}

gradSchemes
{
    default         Gauss linear;
}

divSchemes
{
    default         none;
    div(phi,T)      Gauss linearUpwind grad(T);
}

laplacianSchemes
{
    default         none;
    laplacian(DT,T) Gauss linear corrected;
}

interpolationSchemes
{
    default         linear;
}

snGradSchemes
{
    default         corrected;
}


// ************************************************************************* //
```

Figure 41 fvSchemes

4.2.4.3. Peclet Number

The parameter that basically controls the diffusive behavior in the interior of the grid is the Peclet number.

$$Pe = \frac{u*L}{D\tau} \qquad \textit{Equation 42}$$

It is evident that the value of the transfer coefficient increases by increasing Peclet number because the latter depends on the value of the diffusion coefficient, which increases with a decreasing Peclet number.

In our case, in which we already have defined the parameters above, the Peclet number is computed from the equation below:

$$Pe = \frac{u*L}{D\tau} = \frac{0.01*0.01}{0.01} = 0.01 \qquad \textit{Equation 43}$$

4.2.4.4. Results

In our case, we will study the effect of the Peclet number which implies the effect of the diffusion coefficient of the tracer which is stored in the transportProperties /constant folder, as we already mentioned.

Three simulations will be done with three different diffusion coefficients and, as a result, three Peclet numbers.

In this thesis, the results of velocity field are shown in the previous section throughout the entire geometry for the simpleFoam simulation. In this section the distribution of the tracer concentration will be presented graphically for scalarTransportFoam simulations during the tracer was injected.

Simulation 1

Firstly, the distribution of the tracer concentration inside the grid will be researched, when the tracer was injected using the value of velocity field derived from the simpleFoam simulation. Also, the value of concentration field acquired from the first scalarTransportFoam simulation for the T field was used with a diffusion coefficient equal to 0.01 which leads to a Peclet number = 0.01.

The time required for the tracer to be transferred to the output of the grid based on the above boundary conditions is estimated at 0.065 s after many tests in OpenFoam /scalarTransportFoam solver.

The time step is dt = 0.0005 and as a result the time steps which are depicted on the x-axis (horizontal) in the figure below are:

$$time_{steps} = \frac{end_{time} - start_{time}}{dt} = \frac{0.065}{0.0005} = 130 \quad \textit{Equation 44}$$

The diagram below shows the concentrations taken for each time step at the output, divided by an average patch area A = 10^{-6}, since the concentration may not be the same everywhere because of different flow velocities.

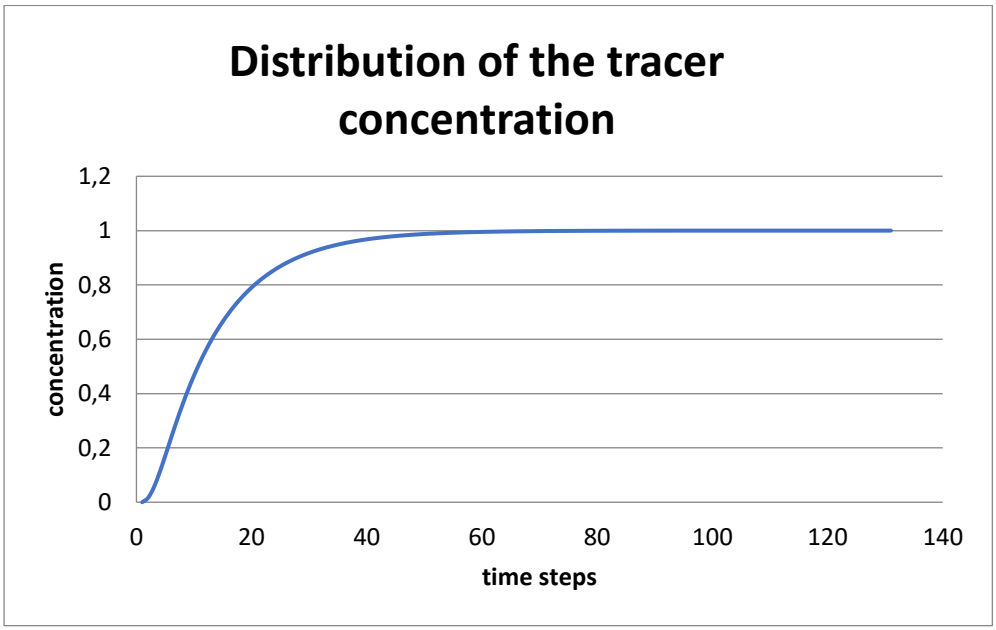

Figure 42 Tracer concentration of the first simulation

Furthermore, a second diagram could be plotted to evaluate the residence time distribution (RTD) which results from differences in concentration between time steps.

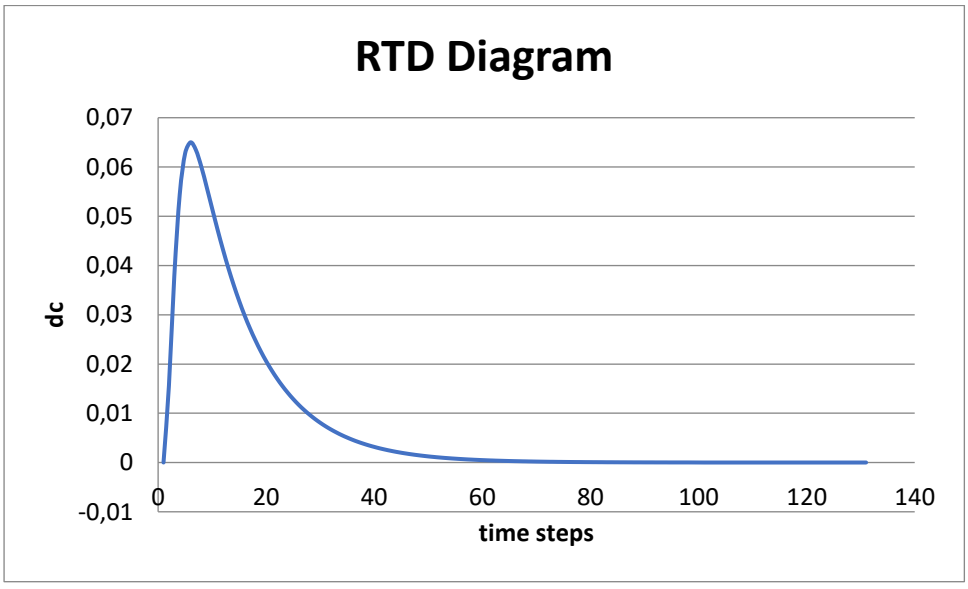

Figure 43 RTD Diagram of the first simulation

Simulation 2

Subsequently, the second simulation concerns to a diffusion number Dτ = 0.0001 which leads to a Peclet number:

$$Pe = \frac{u*L}{Dt} = \frac{0.01*0.01}{0.0001} = 1 \qquad \textit{Equation 45}$$

The time calculated in this case that the substance needs to be transported at the output of the gird is estimated at approximately 1.8 s.

$$time_{steps} = \frac{end_{time} - start_{time}}{dt} = \frac{1.8}{0.1} = 18 \qquad \textit{Equation 46}$$

The change of the diffusion coefficient of the tracer is stored in the transportProperties /constant folder, as we already mentioned is depicted below.

```
/*--------------------------------*- C++ -*----------------------------------*\
  =========                 |
  \\      / F ield        | OpenFOAM: The Open Source CFD Toolbox
   \\    /  O peration     | Website:  https://openfoam.org
    \\  /   A nd          | Version:  8
     \\/    M anipulation  |
\*---------------------------------------------------------------------------*/
FoamFile
{
    version     2.0;
    format      ascii;
    class       dictionary;
    location    "constant";
    object      transportProperties;
}
// * * * * * * * * * * * * * * * * * * * * * * * * * * * * * * * * * * * * //

DT          DT [0 2 -1 0 0 0 0] 0.0001;


// ************************************************************************* //
```

Figure 44 Change of Diffusion Coefficient in the second simulation

The tracer's concentration distribution as well as the RTD diagram is shown below:

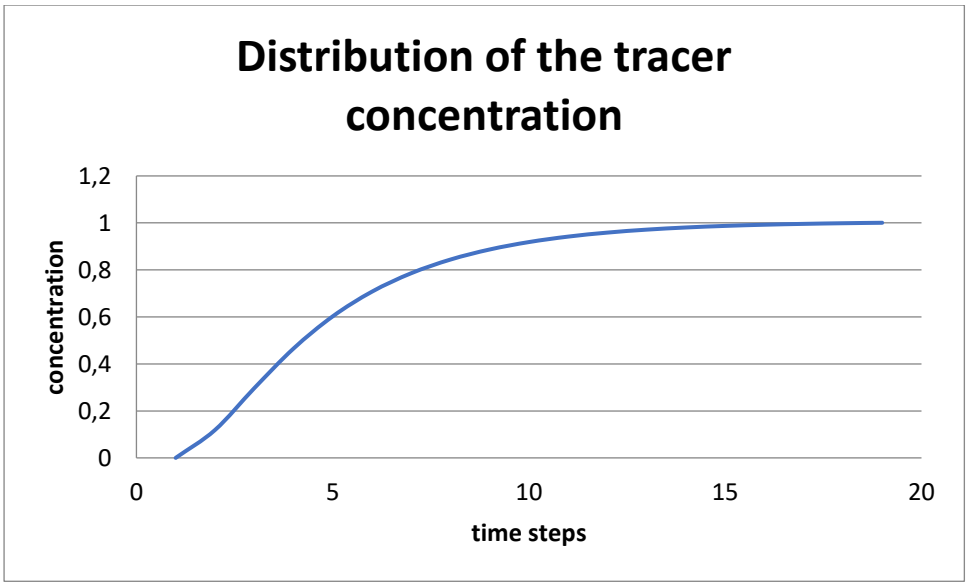

Figure 45 Tracer concentration of the second simulation

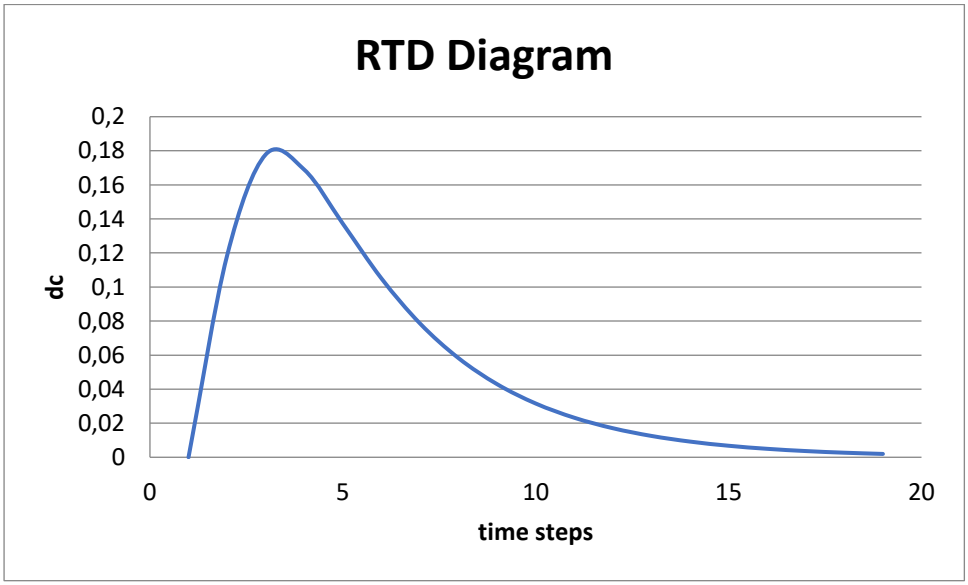

Figure 46 RTD Diagram of the second simulation

Simulation 3

Finally, a third simulation will be conducted with an even smaller diffusion coefficient equaling Dτ =0.000001 which leads to a Peclet number:

$$Pe = \frac{u*L}{Dt} = \frac{0.01*0.01}{0.000001} = 100 \qquad \textit{Equation 47}$$

The time calculated needed in this case to transport the substance to the output of the system is estimated at 2.2 s. The time step is dt = 0.1, so the time steps recorded on the x-axis (horizontal) are:

$$time_{steps} = \frac{end_{time} - start_{time}}{dt} = \frac{2.2}{0.1} = 22 \qquad \textit{Equation 48}$$

The changes of the diffusion coefficient of the tracer as well as the new ControlDict dictionary are depicted below:

```
/*--------------------------------*- C++ -*----------------------------------*\
  =========                 |
  \\      / F ield        | OpenFOAM: The Open Source CFD Toolbox
   \\    /  O peration     | Website:  https://openfoam.org
    \\  /   A nd          | Version:  8
     \\/    M anipulation  |
\*---------------------------------------------------------------------------*/
FoamFile
{
    version     2.0;
    format      ascii;
    class       dictionary;
    location    "constant";
    object      transportProperties;
}
// * * * * * * * * * * * * * * * * * * * * * * * * * * * * * * * * * * * * //

DT          DT [0 2 -1 0 0 0 0] 0.000001;

// ************************************************************************* //
```

Figure 47 Change of Diffusion Coefficient in the third simulation

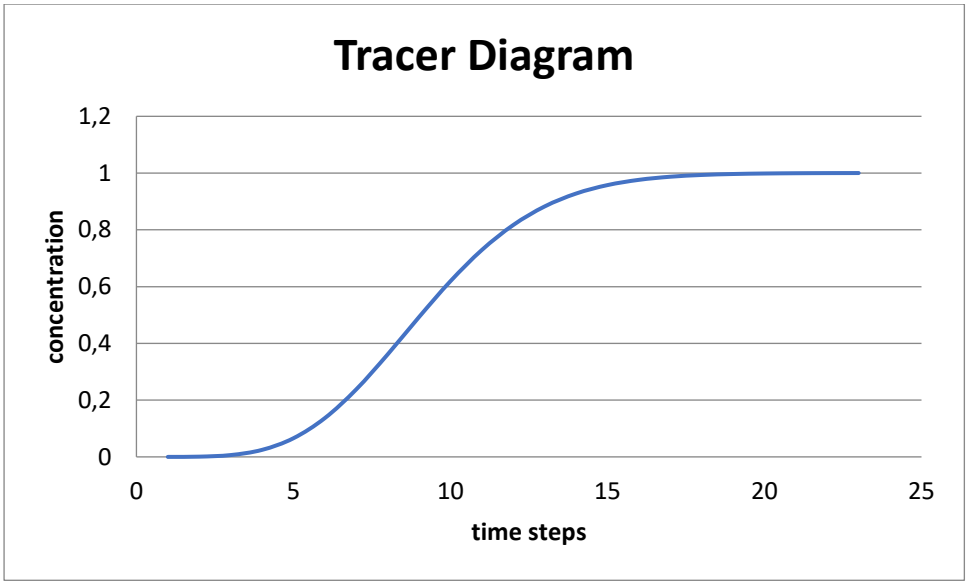

Figure 48 Tracer concentration of the third simulation

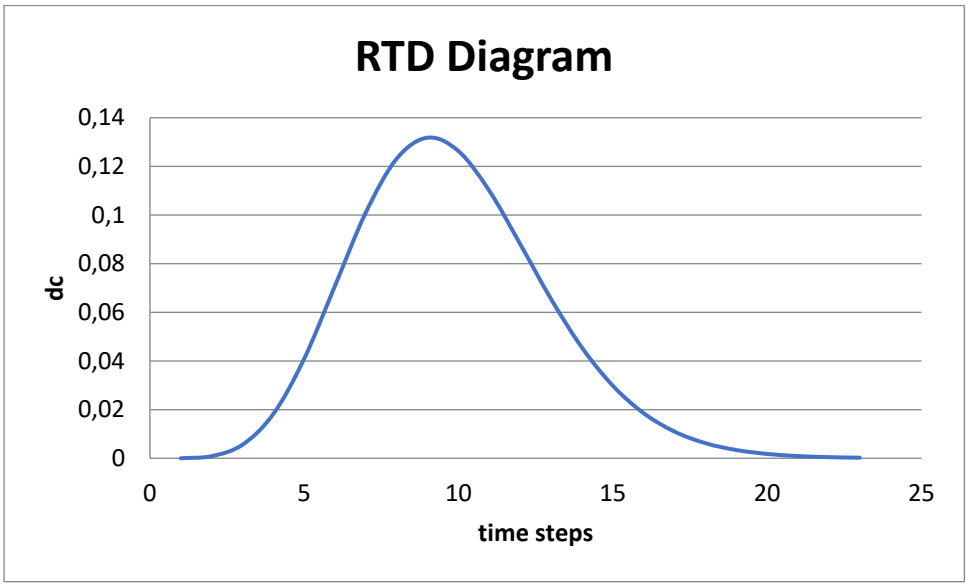

Figure 49 RTD Diagram of the third simulation

4.3. Second Case

The aim of this thesis is to study the transport through fibrous media. In this context, we are interested to see how the response of a fibrous medium to a step-change in inlet concentration, is affected by its microstructure, specifically the effect of volume fraction and Peclet number.

The first case which had been presented in detail in the previous section describes the simulations done with the help of SimpleFoam & ScalarTransporFoam solver to study the transport as well as the effect of the diffusion number.

A second case will be conducted with a different volume fraction. As we already mentioned, the volume fraction in the first case is equal to ϕ=0.2. For the second case, all the other parameters will remain constant and only the volume fraction will be defined with a value of ϕ = 0.4.

The same procedure will be followed exactly as previously, and the results will be presented below.

4.3.1. Geometry & Mesh

The geometry of our simulation was made in the Gmsh program. The below grid consists of 500 fibers with a radius of r=0.015554, volume fraction = 0.4 and a safe distance between the fibers=1.5. The length and the height of the grid is 1 cm while the depth is set to W = 0.001 (directions x, y, and z in the Cartesian coordinates, respectively). Fluid flow in this geometry is considered as 2D from the left side to the right one with a velocity equal to 0.01 m/s.

The physical groups needed for subsequent modeling as well as the parameters needed to carry out the correct meshing remain the same as previously in the first case.

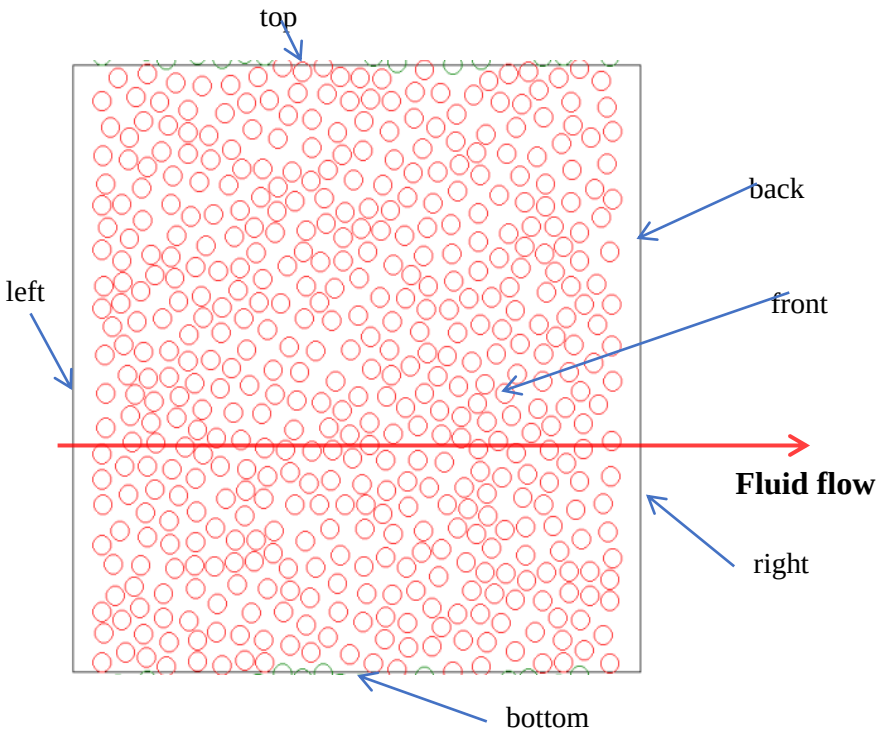

Figure 50 Fiber Distribution

The below figures depict the result of the meshed grid as well as the statistics of this case.

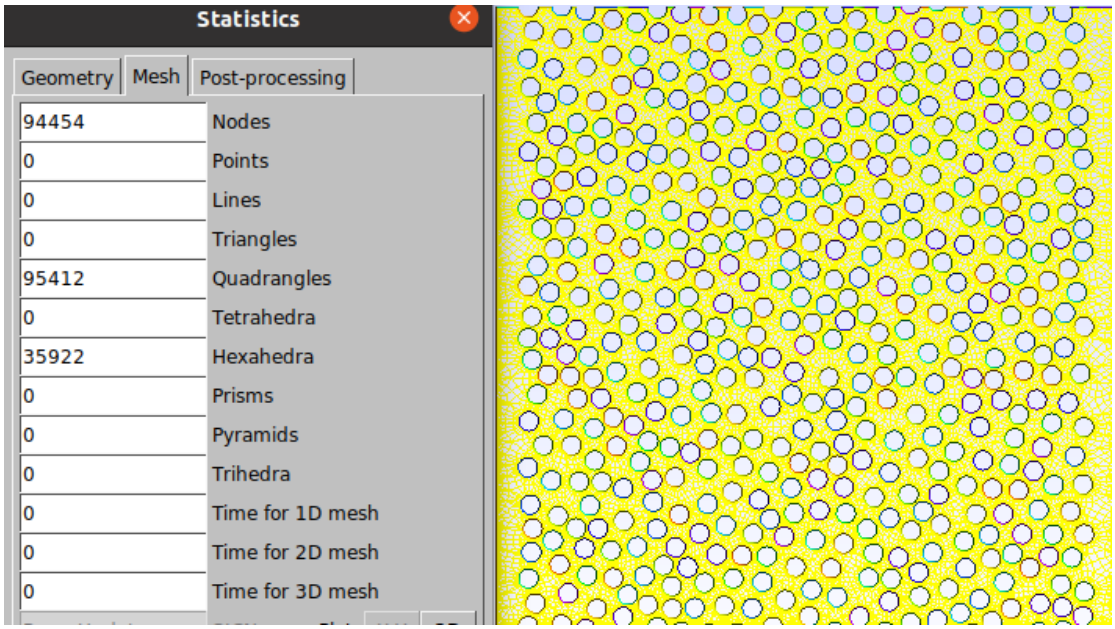

Figure 51 Statistics of the grid

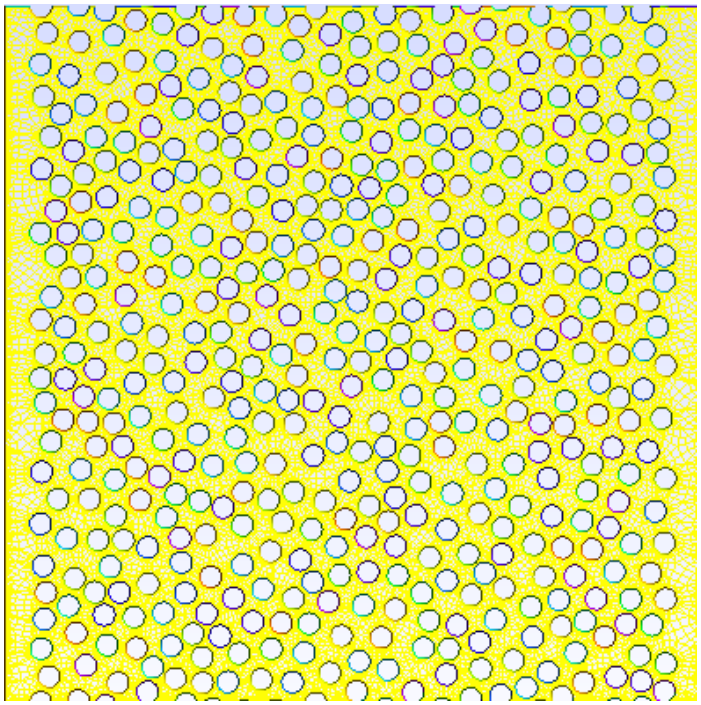

Figure 52 Final grid

4.3.2. Results

4.3.2.1. SimpleFoam

After the simulation, Openfoam calculates the value of the flow rate (Q) which, in our case, equals to Q= $9.9998*10^{-9}$ m^3/s.

Also, the value of the average patch area is A = 0.01(y) *0.0001(z) =10^{-6} m^2 as we mentioned in the first case.

Finally, the average value of the velocity is calculated at the price of:

$$uavg = \frac{Q}{A} = 9.9998 * 10^{-3}\ m/s \qquad \textit{Equation 49}$$

The number of Reynolds once again confirms the choice of simplefoam as the most appropriate choice because:

$$Re = \frac{uavg * Dfiber}{v} = 308 \ \textit{(Laminar flow)} \qquad \textit{Equation 50}$$

- U_{avg} = 9.9998 *10^{-3} m/s
- D_{fiber}= 0.031108 m
- V=10^{-6} m^2/s^2

4.3.2.2. Paraview

In order to view the case files and results graphically, the below figures show the workbench of ParaView 5.6.0 that was used for post processing for this thesis work.

A sample of how the results can be viewed is seen in the below figures which depict the velocity profile at the end of the grid.

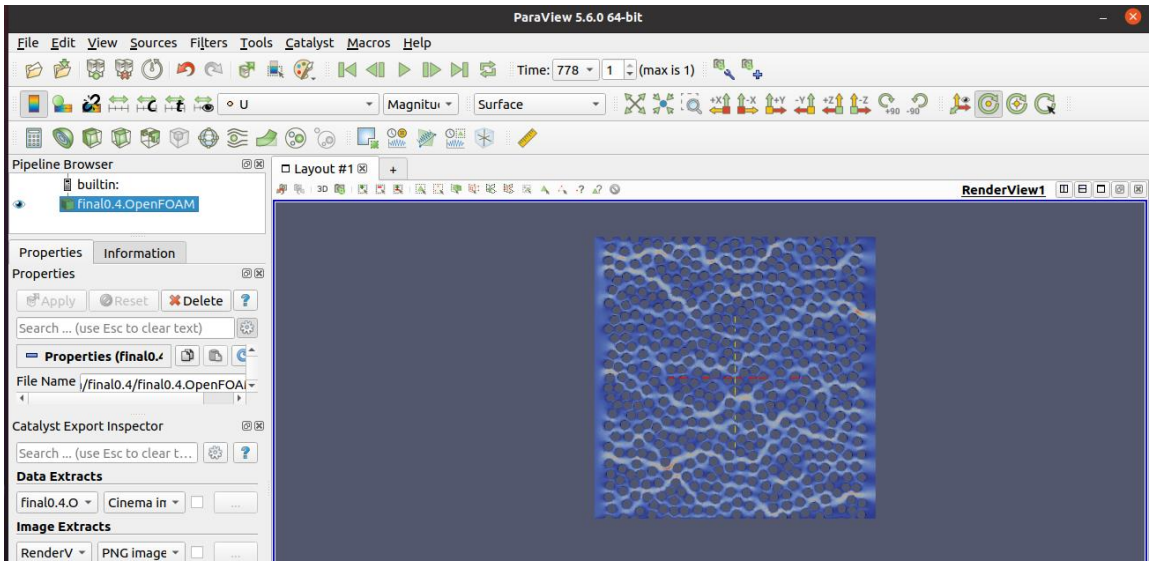

Figure 53 Velocity Profile (1)

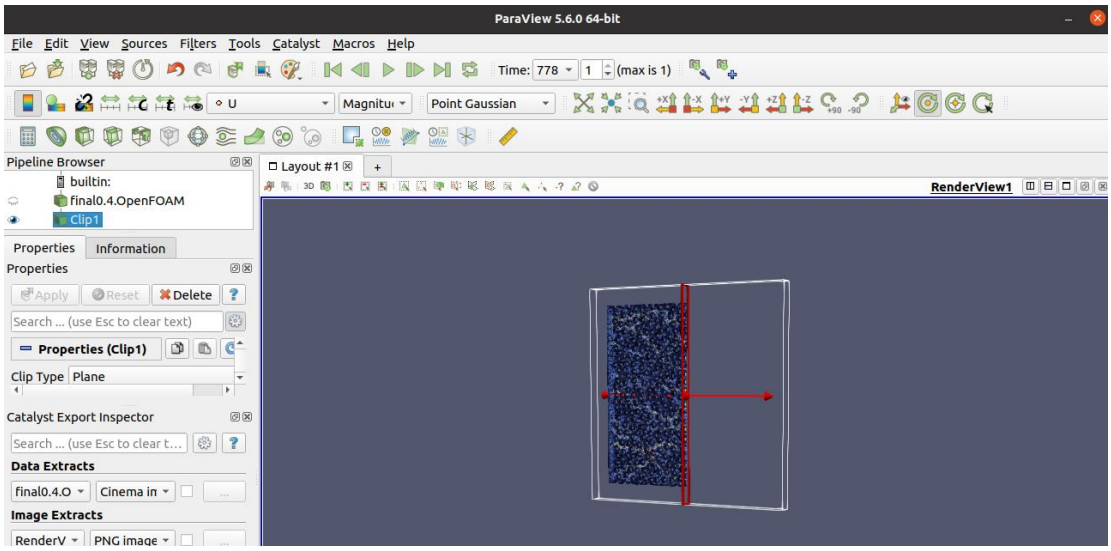

Figure 54 Velocity Profile (2)

4.3.3. Residence Time Distribution (RTD)

4.3.3.1. Results

In the second case, the effect of the Peclet number which implies the effect of the diffusion coefficient of the tracer will be studied, as previous.

The boundary conditions as well as the 0/constant/system folders remain the same with the only difference of the velocity field.

The final result of velocity field is shown in the previous section throughout the entire geometry for the simpleFoam simulation with a volume fraction (ϕ) equal to 0.4.

Three simulations will be done with three different diffusion coefficients and, as a result, three Peclet numbers.

$$\mathrm{Pe} = \frac{u * L}{\mathrm{D}\tau} = \frac{0.01 * 0.01}{0.01} = 0.01 \ \ (simulation\ 1)$$

$$\mathrm{Pe} = \frac{u * L}{\mathrm{D}\tau} = \frac{0.01 * 0.01}{0.0001} = 1 \ \ (simulation\ 2)$$

$$\mathrm{Pe} = \frac{u * L}{\mathrm{D}\tau} = \frac{0.01 * 0.01}{0.000001} = 100 \ \ (simulation\ 3\ )$$

In this section the distribution of the tracer concentration and the Residence Time Distribution (RTD) diagrams will be presented graphically for scalarTransportFoam simulations during the tracer was injected.

Simulation 1

With a Peclet number equal to 0.01, the time required for the tracer to be transferred to the output of the grid based on the above boundary conditions is estimated at 0.085 s after many tests in openfoam /scalarTransportFoam solver.

$$time_{steps} = \frac{end_{time} - start_{time}}{dt} = \frac{0.085}{0.005} = 17 \qquad \textit{Equation 51}$$

The diagram below shows the concentrations taken for each time step at the output, divided by an average patch area A = 10^{-6}, since the concentration may not be the same everywhere because of different flow velocities.

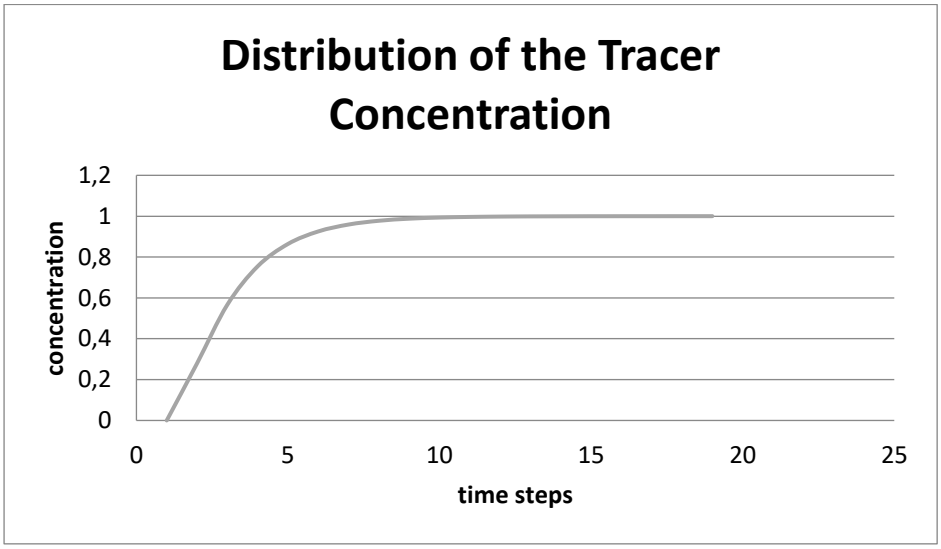

Figure 55 Tracer concentration of the first simulation

Furthermore, a second diagram could be plotted to evaluate the residence time distribution (RTD) which results from differences in concentration between time steps.

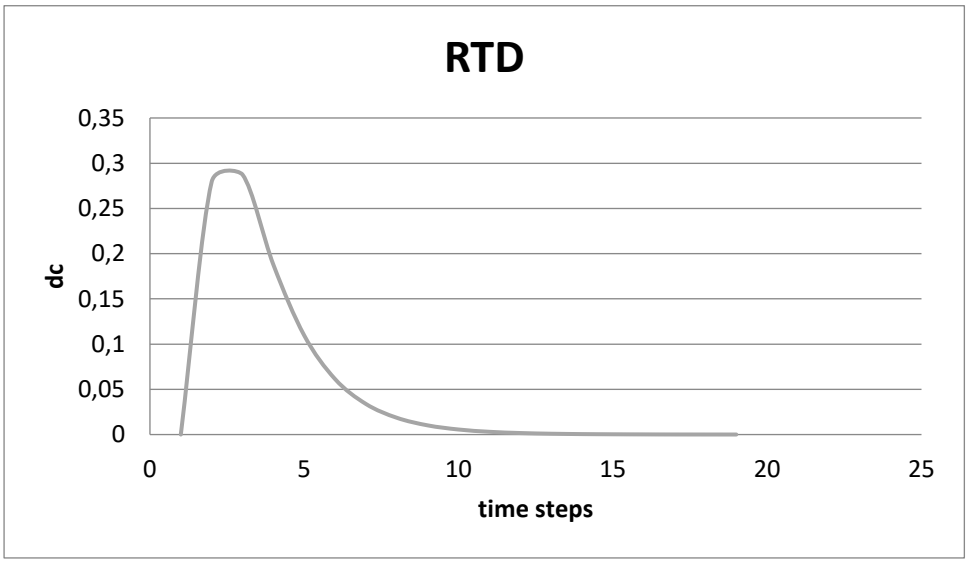

Figure 56 RTD Diagram of the first simulation

Simulation 2

With a Peclet number equal to 1, the time estimated for the tracer to be transferred is 2.2 s.

$$time_{steps} = \frac{end_{time} - start_{time}}{dt} = \frac{2.2}{0.1} = 22 \qquad \textit{Equation 52}$$

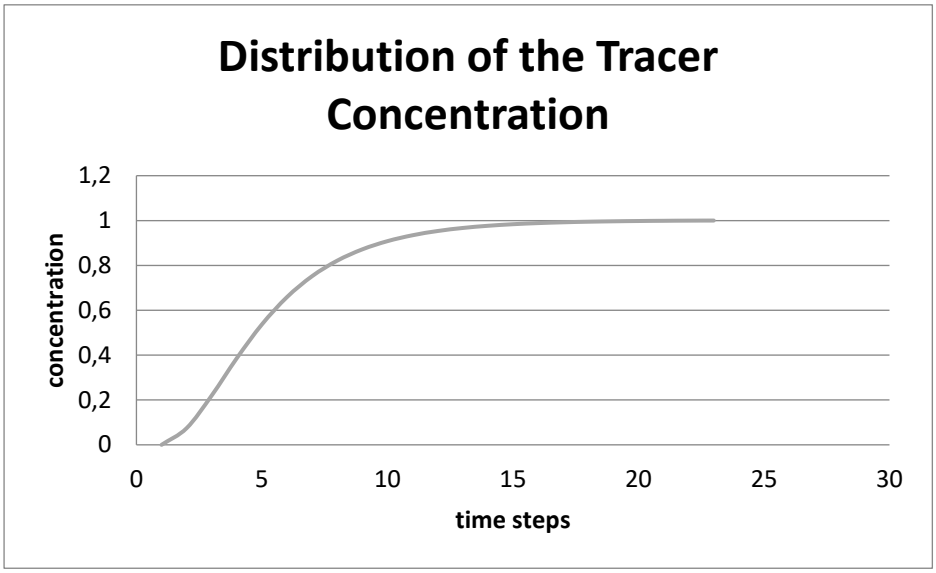

Figure 57 Tracer concentration of the second simulation

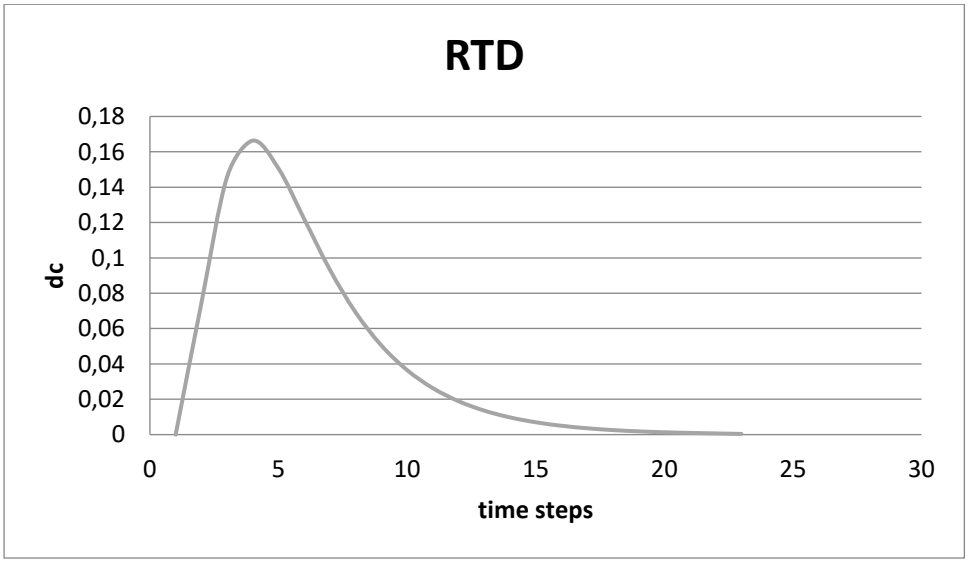

Figure 58 RTD Diagram of the second simulation

Simulation 3

Finally, with a Peclet number equal to 100 the time required is 2.2 s for the tracer to be transferred at the end of the grid and the total time steps are:

$$time_{steps} = \frac{end_{time} - start_{time}}{dt} = \frac{2.2}{0.1} = 22 \qquad \textit{Equation 53}$$

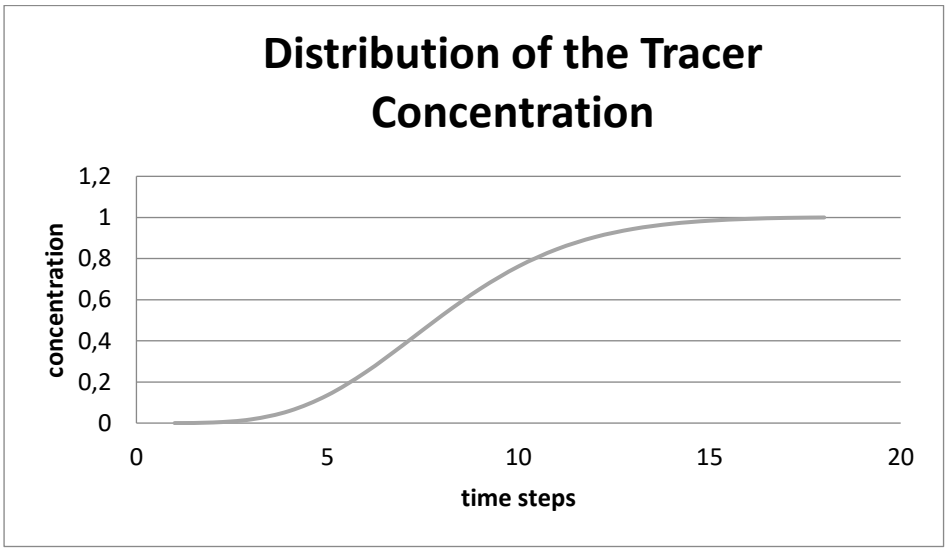

Figure 59 Tracer concentration of the third simulation

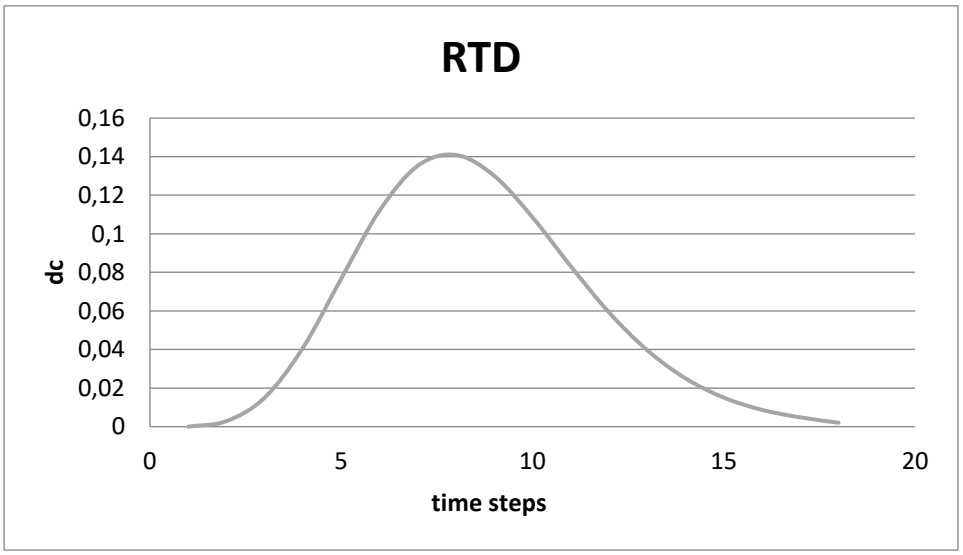

Figure 60 RTD Diagram of the third simulation

4.4. Conclusions & Future Work

The design of the tracer injection was conducted by computation of fluid dynamics modeling. Two cases were studied with the same boundary conditions but a different volume fraction. The two models contained two parts; firstly, velocity was calculated using the simpleFoam solver and then transport of the tracer (passive scalar) was evaluated using the scalarTransportFoam solver for three different diffusion coefficients for each case.

From the above simulations we can conclude that the value of the diffusion coefficient has a significant effect on the transport of the tracer.

When the Peclet number is small (simulation 1), diffusion must be considered because of the greater impact of the diffusion coefficient compared to the flow velocity. The transfer takes place not only with the velocity of the flow field but also with the diffusion mechanism.

For larger Peclet numbers (simulations 2&3), the diffusion coefficient is decreased significantly and as a result the substance is transported in a much shorter time than it would be transported by diffusion alone.

Also, from the second case we can conclude that volume fraction has an impact on the response of a fibrous medium. As the volume fraction of the fibers increased then the velocity of the fluid decreased, since it had to pass through less available space and the transfer took place in a longer time. As we have already mentioned in the results of previous research, at low porosity levels, the decrease in permeability caused by increased nonuniformity in fiber arrangement. This is not surprising, since researchers have previously shown that fiber clusters can obstruct flow paths and delay flow.

Therefore, many different simulations and tests have been left for the future because of absence of time (for instance, the simulations with real data are very complicated, requiring much time to finish even a unique run due to a grid consists of million cells). Future work needs deeper analysis and work of the transport case as well as a better comprehension of how diffusion and volume fraction can affect the response of a flow through fibrous media. The preparatory results of these experiments do not seem to be sufficient, and deeper analysis is still vital to realize the above techniques.

LITERATURE

[**1**] Ahmed, T. (2011). *Advanced Reservoir Management and Engineering*, Second Edition. 2 Edition. Gulf Professional Publishing.

[**2**] Chawla, K. (2016) Fibrous Materials, pp 11. Cambridge University Press DOI: https://doi.org/10.1017/CBO9781139342520.004

[**3**] Chung, P. (2011) The Holistic Strategy in Multi-Scale Modeling. *Advances in Chemical Engineering Series*

[**4**] Apostal, T. M. (1957). Mathematical Analysis. Addison-Wesley, Reading, Mass., 553 pp., 76s.

[**5**] Bear, Jacob (1960). Thesis (Ph. D. in Civil Engineering), University of California, Berkeley, Sept. 1960.

[**6**] Hilfer, R. (1996). Transport and relaxation phenomena in porous media. Advances in Chemical Physics, 92: 299-424.

[**7**] Kramers, H., Alberda, G. (1953) Frequency response analysis of continuous flow systems. Chemical Engineering Science, 2 (4). 173-181.

[**8**] Clague DS, Kandhai BD, Zhang R (2000). Hydraulic permeability of (un)bounded fibrous media using the lattice Boltzmann method. *Phys Rev E*;61(1): 616–25.

[**9**] DeFrates, K.G.; Moore, R.; Borgesi, J.; Lin, G.; Mulderig, T.; Beachley, V.; Hu, X. (2018) Protein-Based Fiber Materials in Medicine: A Review. *Nanomaterials* , *8*, 457. https://doi.org/10.3390/nano8070457

[**10**] Erisken, C., Tsiantis, A., Papathanasiou, T. D., & Karvelas, E. G. (2020). Collagen fibril diameter distribution affects permeability of ligament tissue: A computational study on healthy and injured tissues. *Computer methods and programs in biomedicine*, *196*, 105554. https://doi.org/10.1016/j.cmpb.2020.105554

[**11**] Figjestol, P., Lewis, R. (1998) *Permeability*. Chemistry of Cement, ch. 12

[**12**] Gebart BR (1992). Permeability of unidirectional reinforcements for RTM. *Journal of Composite Matter,* vol 26

[**13**] Gebart, B. R., & Lidström, P. (1996). *Measurement of in-plane permeability of anisotropic fiber reinforcements. Polymer Composites, 17(1), 43–51.* doi:10.1002/pc.10589

[**14**] Huang X, Wang QH, Zhou W, Li JR (2013) A simple fracture energy prediction method for fiber network based on its morphological features extracted by X-ray tomography. Mater Sci Eng A 585:297–303

[**15**] Huang, X., Zhao, Y., Wang, H. (2017). Investigation of transport property of fibrous media: 3D virtual modeling and permeability calculation. Engineering with Computers 33, 997–1005. https://doi.org/10.1007/s00366-017-0511-4

[**16**] Jaganathan, S., Vahedi Tafreshi, H., & Pourdeyhimi, B. (2008). *A realistic approach for modeling permeability of fibrous media: 3-D imaging coupled with CFD simulation. Chemical Engineering Science, 63(1), 244–252.* doi:10.1016/j.ces.

[**17**] Karakashov, B., Toutain, J., Achchaq, F., Legros, P., Fierro, V., & Celzard, A. (2019). *Permeability of fibrous carbon materials. Journal of Materials Science.* doi:10.1007/s10853-019-03854-5

[**18**] Karvelas, E. G., Tsiantis, A., & Papathanasiou, T. D. (2020). Effect of micropolar fluid properties on the hydraulic permeability of fibrous biomaterials*. Computer Methods and Programs in Biomedicine,* 185, 105135. doi:10.1016/j.cmpb.2019.105135

[**19**] Koponen A, Kandhai D, Hellen E (1998). Permeability of three-dimensional random fiber webs. Phys Rev Lett;80(4):716.

[**20**] Li, J., Ho, M. Wu, L. Zhang, Y. (2016) Lattice Boltzman modelling of Intrinsic permeability. *Cornell University*

[**21**] Liu, H. L., & Hwang, W. R. (2012). *Permeability prediction of fibrous porous media with complex 3D architectures. Composites Part A: Applied Science and Manufacturing, 43(11), 2030–2038.* doi:10.1016/j.compositesa.2012.0

[**22**] Nabovati, A., Llewellin, E. W., & Sousa, A. C. M. (2009). A general model for the permeability of fibrous porous media based on fluid flow simulations using the lattice Boltzmann method. *Composites Part A: Applied Science and Manufacturing, 40(6-7), 860–869.* doi:10.1016/j.compositesa.2009.0

[**23**] Novacovic, G., Altman, G., Horan, R., Kaplan, D. (2004) Tissue Engineering of Ligaments. *Annual Review of Biomedical Engineering*

[**24**] Patiño, Iván, Vargas, Carlos, & Vanegas, Juan. (2014). Methods for permeability measurements of fibrous reinforced preforms. *Revista Facultad de Ingeniería Universidad de Antioquia*,(72),186-2002.RetrievedOctober 03, 2021, from http://www.scielo.org.co/scielo.php?script=sci_arttext&pid=S0120-62302014000300016&lng=en&tlng=en.

[**25**] Shou, D., Fan, J., & Ding, F. (2011). Hydraulic permeability of fibrous porous media*. International Journal of Heat and Mass Transfer, 54(17-18), 4009–4018.* doi:10.1016

[**26**] Spielman L, Goren SL (1986) Model for predicting pressure drop and filtration efficiency in fibrous media. Environ Sci Technol 2:279–287

[**27**] Stylianopoulos T, Yeckel A, Derby JJ, Luo XJ, Shephard MS, Sander EA, Barocas VH (2008) Permeability calculations in three-dimensional isotropic and oriented fiber networks. Phys Fluids 20:123601

[**28**] Abstract, M. T. (2009). A Hardware Accelerator for the OpenFoam Sparse Matrix-Vector Product. http://ce.et.tudelft.nl/2009

[**29**] Horvat, M. (2016). MASTER'S THESIS. A study of rotor-stator interaction models for numerical performance prediction of centrifugal pumps.

[**30**] Mekonnen, A. T. (2016). Modelling a tracer injection and sensor manifold.

[**31**] Mona Nakhostin, S., & Erik Teigen Giljarhus Muk Chen Ong, K. (2019). MASTER'S THESIS. Investigation of transitional turbulence models to predict drag crisis for flow over spheres and cylinder

[**32**] Prakash Reddy Samala, B., & Mellibovsky Josep Maria Bergadà, F. (2015). MASTER THESIS Computational Investigation of Active Flow Control Parameters on the Aerodynamic Performance of NACA 2412 Airfoil.

[**33**] Sihvo, C. (2014). MASTER'S THESIS Numerical Method for Shape Optimization from Wind Noise Perspective.

[**34**] Tutorial Ten Residence Time Distribution. (2018). www.cfd.at

[**35**] Verclyte, A. (2012-2013). Faculteit Bio-ingenieurswetenschappen Mass and heat transfer modelling in screw reactors.

[**36**] Winter, M. (2013). Benchmark and validation of Open Source CFD codes, with focus on compressible and rotating capabilities, for integration on the SimScale platform.

[**37**] S. Sumbekova, A. Iskakova, and A. Papathanasiou, "Microstructural clustering in multiphase materials and its quantification," *Phys. A Stat. Mech. its Appl.*, vol. 532, p. 121809, 2019, doi: 10.1016/j.physa.2019.121809.

[38] Chen, X., & Papathanasiou, T. D. (2007). Micro-scale modeling of axial flow through unidirectional disordered fiber arrays. Composites Science and Technology, 67(7–8), 1286–1293. https://doi.org/10.1016/j.compscitech.2006.10.011

[39] Chen, X., & Papathanasiou, T. D. (2006). On the variability of the Kozeny constant for saturated flow across unidirectional disordered fiber arrays. Composites Part A: Applied Science and Manufacturing, 37(6 SPEC. ISS.), 836–846. https://doi.org/10.1016/j.compositesa.2005.01.018

[40] Åström, B. T., Pipes, R. B., & Advani, S. G. (1992). On Flow through Aligned Fiber Beds and Its Application to Composites Processing. Journal of Composite Materials, 26(9), 1351–1373. https://doi.org/10.1177/002199839202600907

[**41**] Papathanasiou, T. D. (1996). A structure-oriented micromechanical model for viscous flow through square arrays of fibre clusters. *Composites Science and Technology*, *56*(9), 1055–1069. https://doi.org/10.1016/0266-3538(96)00066-8

[42] Bruschke, M. V, & Advani, S. G. (2017). Flow of generalized Newtonian fluids across a periodic array of cylinders Flow of generalized Newtonian fluids across a periodic array of cylinders. 479(1993). https://doi.org/10.1122/1.550455

[43] Skartsis, L., Khomami, B., & Kardos, J. L. (1992). Resin Flow Through Fiber Beds During Composite Manufacturing Processes. Part II: Numerical and Experimental Studies of Newtonian Flow Through Ideal and Actual Fiber Beds. 32(4), 231–239.

[**44**]Carman, B. P. C., & Graduate, P. D. (1932). FLUID FLOW THROUGH GRANULAR BEDS *. *Chemical Engineering Research and Design*, *75*, S32–S48. https://doi.org/10.1016/S0263-8762(97)80003-2

[**45**] Sangani, A. S., & Acrivos, A. (1982). Slow flow past periodic arrays of cylinders with application to heat transfer. International Journal of Multiphase Flow, 8(3), 193–206. https://doi.org/10.1016/0301-9322(82)90029-5